(2)

253805-1-F

Final Report
COMMUNICATION, TRACKING, AND IMAGING SYSTEM RESEARCH

J.S. Accetta
R.C. Anderson
E.L. Johansen
N.S. Subotic
Optical and IR Science Laboratory
Advanced Concepts Division

FEBRUARY 1994

Submitted to:
Naval Air Warfare Center
Aircraft Division
Code PD 35, Bldg. 562
Lakehurst, NJ 08733

Attention: Mr. Michael Jones

Contract Number: DLA900-88-D-0392, D.O.#44

ERIM
P.O. Box 134001
Ann Arbor, MI 48113-4001

ERIM-320

REPORT DOCUMENTATION PAGE

Form Approved
OMB No. 0704-0188

1. AGENCY USE ONLY (*Leave Blank*)	2. REPORT DATE	3. REPORT TYPE AND DATES COVERED
	February 1994	Final Report 5/19/93 - 1/31/94

4. TITLE AND SUBTITLE
Communication, Tracking, and Imaging System Research

5. FUNDING NUMBERS
DLA900-88-0392, D.O. #44

6. AUTHOR(S)
J.S. Accetta, R.C. Anderson, E.L. Johansen and N.S. Subotic

7. PERFORMING ORGANIZATION NAME(S) AND ADDRESS(ES)
Environmental Research Institute of Michigan
P.O. Box 134001
Ann Arbor, MI 48113-4001

8. PERFORMING ORGANIZATION REPORT NUMBER
253805-1-F

9. SPONSORING/MONITORING AGENCY NAME(S) AND ADDRESS(ES)
Naval Air Warfare Center
Aircraft Division
Code PD 35, Bldg. 562
Lakehurst, NJ 08733

10. SPONSORING/MONITORING AGENCY REPORT NUMBER

11. SUPPLEMENTARY NOTES

12a. DISTRIBUTION/AVAILABILITY STATEMENT
Unlimited

12b. DISTRIBUTION CODE

13. ABSTRACT (*Maximum 200 words*)

This report summarizes research supporting communication, tracking and imaging systems. Four specific topics were addressed during this study:

Active Communication Systems: Communications between incoming aircraft and carrier air traffic control are normally by radio and visual landing aids, which are not available during EMCON conditions. Several potential low probability of intercept communication systems were conceptualized and analyzed.

Spread Spectrum Tracking: The objective of this task was an assessment of various approaches for aircraft tracking based on spread spectrum technology for reducing the probability of intercept. Two specific transmit receive architectures were examined: 1) beacon on aircraft; and 2) spread spectrum waveform from a range/Doppler radar on board ship.

MMW Imaging Evaluation: Millimeter wave imaging system capabilities are progressing rapidly. A survey of current and projected MMW imaging capabilities was conducted, identifying several potential systems.

Wind Detection: A current interest of the Navy is the remote detection of wind vectors around carriers and other aviation-capable ships. Microwave radar sensing of the flowfield is one possible approach. This study shows that, because of the very low backscatter from atmospheric constituents, very high transmitter power would be required to achieve acceptable signal to noise levels.

14. SUBJECT TERMS	15. NUMBER OF PAGES
	92
	16. PRICE CODE

17. SECURITY CLASSIFICATION OF REPORT	18. SECURITY CLASSIFICATION OF THIS PAGE	19. SECURITY CLASSIFICATION OF ABSTRACT	20. LIMITATION OF ABSTRACT
Unclassified	Unclassified	Unclassified	Unlimited

CONTENTS

CONTENTS (Continued)

CONTENTS (Continued)

FIGURES

FIGURES (Continued)

TABLES

1.0 INTRODUCTION AND SUMMARY

This report summarizes technical activity performed by the Environmental Research Institute of Michigan for the Naval Air Warfare Center, Lakehurst. The technical effort was performed over the period 18 May to 31 December 1993. This effort consisted of eight tasks. These are listed below with a brief statement of summary and conclusions. The remainder of the report consists of full discussions of Tasks 5 through 8.

1.1 ANALYSIS OF CATAPULT INFRARED EMISSIONS

Carrier catapult tracks, steam vents, and related machinery are maintained at high temperature during flight operations. These components may enhance the general detectability of the carrier to infrared sensors, reducing the survivability of the ship.

1.2 SUPPORT TO EO LAUNCH AND RECOVERY EQUIPMENT

Aircraft carrier arresting engines, wires, and related components absorb a great deal of energy during aircraft recovery operations. These components may enhance the overall detectability of the carrier to infrared sensors, reducing the survivability of the ship.

1.3 INFRARED IMAGING SYSTEM INSTRUCTION

Infrared systems are becoming increasingly common in US and foreign military service. However, the images provided by these devices are subject to misinterpretation unless the underlying phenomena are understood.

1.4 BINARY OPTICS INSTRUCTION

The use of binary optics is expected to grow explosively during the next decade. This important technology area can provide significantly greater capability to military systems if the fundamentals are understood by decision makers.

1.5 ACTIVE COMMUNICATION SYSTEMS

Communications between incoming aircraft and carrier air traffic control are normally by radio and visual landing aids. During EMCON conditions, conventional approach radar and radio communications are unavailable. This impedes the normal landing flow. Generally, the hazard levels are increased, and normal sequencing of bolter traffic is more difficult.

A number of potential communication systems were conceptualized during this study, providing a range of solutions from low to high risk, and low to high performance.

1.6 RESEARCH ON TRACKING AIRCRAFT USING SPREAD SPECTRUM TECHNOLOGY

Spread spectrum techniques promise to allow covert tracking of air vehicles. These systems have not yet been evaluated with respect to their performance of carrier flight operations supporting tasks.

We have found that bandpass requirements to achieve low main beam detection are quite high and probably not achievable at X band. However, use of higher frequencies or power management should greatly reduce the bandpass requirement. Also, the threat assumptions overstate the system requirements. A more thorough threat assessment may provide more relaxed X band requirements.

1.7 MMW IMAGING EVALUATION

Millimeter wave imaging systems are progressing rapidly. A survey of current and projected MMW imaging capabilities will provide a strong foundation for future development and integration decisions.

A number of systems are available with the potential for MMW imaging of approaching aircraft. Geometric constraints limit the performance of ISAR processing, however. Additional data are needed to assess the potential of this technique. In particular, aircraft motion during approach is a particularly valuable parameter.

1.8 WIND DETECTION

A current interest of the Navy is the remote detection of wind vectors around carriers and other aviation-capable ships. Accurate information of the flow vectors to ranges approaching one-quarter mile would aid in the recovery of aircraft.

Use of radar for wind detection is hampered by the very low reflectance of the atmosphere in available bands. This in turn required a very powerful radar which will be difficult to implement aboard ship.

2.0 TASK 5: ACTIVE COMMUNICATION SYSTEMS

2.1 INTRODUCTION AND SUMMARY

The objective of task 5 of this effort is the investigation of novel active communication between US naval aircraft and aircraft carriers during the aircraft recovery cycle. Novel in this instance means other than conventional radio or radar, the principal consideration being the ability to achieve covert communication and avoid hostile intercept during EMCON operations. The upper limit of probability of intercept (POI) was not specified; thus there is no attempt to define and examine concepts meeting a specific POI. The approach taken was to look at concepts with intrinsically low POIs. The operational constraints were taken to be effective communication range to five kilometers in nominal weather and deviation from flight path of less than five degrees.

Active electro-optical systems operating above the near infrared region of the spectrum offer potential solutions to the low POI communications problem in three respects:

- operation outside the visible region of the spectrum offers day/night operation without risk of visible intercept
- the narrow beamwidths obtainable in the optical portion of the spectrum (as opposed to microwave) afford an intrinsically low POI
- characteristic atmospheric attenuation naturally limits the range of useful signal intercept.

The additional requirement of eye-safe operation generally limits operation to wavelengths greater than 1.5 μm; however, in those cases with exceptionally low power requirements, operation could be extended to shorter wavelengths. Explicit consideration of eye safety requirements for the sources employed has not yet been accomplished.

Cost, complexity, the difficulties of attempting to modify aircraft, and near term availability of the technology and devices were considered in the evaluation of the various concepts, at least in a qualitative manner.

Within the technical and fiscal constraints specified above and with some reasonable assumptions, we have found that there are several viable concepts that employ available optical communications technology and devices.

2.2 CONCEPT ANALYSIS

2.2.1 System Performance Estimates

SNR Analysis

It is instructive to examine configuration performance by casting the SNR equation into a form that enables the assessment of the individual effects. The signal to noise power ratio is the mean square to variance ratio of the signal current. Thus

$$SNR = \frac{\langle I_s \rangle^2}{\sigma_{Is}^2}$$

If we assert that the individual effects that contribute to the variance are statistically independent, then:

$$SNR = \frac{\langle I_s^2 \rangle}{\sigma_1^2 + \sigma_2^2 + \sigma_n^2}$$

which can be expressed as

$$SNR = \frac{1}{\frac{1}{SNR_1} + \text{----} + \frac{1}{SNR_n}}$$

The various components are considered as follows:

Shot Noise

$$SNR_1 = \beta P_s / 2qFB$$

β = Current Unit Gain Responsivity

P_s = Received Signal Power

q = Electronic Charge

F = Excess Noise Factor

B = Electrical Bandwidth

F is dependent upon detector type but typical values are:

F = 1.0 for photodiodes

= 1.3 for photomultipliers

= 2 for photoconductors

> 2 for avalanche photodiodes (2.4 at 1.06 μm and 5.5 at 1.53 μm for Si)

Background Noise

$$SNR_2 = \beta P_s^2 K_e^2 / 2qFBP_b$$

where

K_e = Electrical efficiency ($\sim$.6 for single pole filter)

P_B = Background power incident on detector (defined subsequently)

Detector Dark Current

$$SNR_3 = B^2 P_s^2 / (2qFBI_d)$$

where I_d = RMS detector dark current

Thermal Noise

$$SNR_4 = G^2 \beta^2 P_s^2 R_l / (4K_B TB)$$

where

G = Detector gain

R = Load resistor

K_B= Boltzmann's constant

T = Resistor temperature

Pre-Amplifier Noise

$$SNR_5 = G^2\beta^2 P_s^2 / (2qI_aB)$$

where I_a = RMS preamplifier noise current

Laser Amplitude Fluctuations

$$SNR_6 = \frac{1}{\sigma_L^2}$$

where σ_L = Normalized standard deviation of laser output power

Speckle Noise Including Aperture Averaging

$$SNR_7 = \frac{1}{\sigma_{SA}^2}$$

where $\sigma_s^2 \approx \sigma_s^2 \pi (1.2\lambda R/\sigma_{cs})^2/4A$

where

σ_s^2 = Normalized variance of speckle (=1 for fully developed speckle)

λ = Wavelength

R = Range

σ_{cs} = Target cross section

A = Area of the aperture

Cross Section Variation

$$SNR_8 = \frac{1}{\sigma_{cs}^2}$$

where σ_{cs} = Normalized standard deviation of target cross-section

Scintillation Including Aperture Averaging

$$SNR_9 = 1/\phi(e^{\sigma_{lnI}^2 - 1})$$

where

$$\sigma_{lnI}^2 = 1.23\ C_n^2 \left[\frac{2\pi}{\lambda}\right]^{7/6} R^{11/6}$$

C_n^2 = Atmospheric turbulence constant

$$\phi = 4r_o^2/D^2$$

$$r = 2.53\ (C_n^2)^{-3/5} k^{-6/5} R^{-3/5}$$

The conditions limiting aperture averaging and saturation are

if $\phi \geq 1$, then $\phi = 1$

and if $\sigma_{lnI}^2 \geq 10$, then $\sigma_{lnI}^2 = 10$

Backscatter

$$SNR_{10} = \beta P_s^2 K_e^2 / 2qFBP_{BS}$$

where P_{BS} = Backscatter laser power defined below

Background Power

$$P_{BB} = L_B A \theta^2 \epsilon (\lambda/100)$$

where L_B = Background spectral radiance

θ = Receiver FOV (1/2 angle)

ϵ = Optical efficiency

Signal Power

$$P_s = \frac{P_L K_e \sigma_{cs} A \epsilon}{\pi \theta^2 R^4} e^{-2\alpha R}$$

where

P_L = Laser power

α = Atmospheric absorption coefficient

Backscattered Power

$$P_{BS} = \frac{P_L \sigma_{BS} A \epsilon}{R^2} \left[\frac{c t_p}{2} \right] \exp\{-2\alpha R\}$$

where

σ_{BS} = Backscatter coefficient

c = Velocity of light

t_p = Pulse length

Pulse Averaging

$SNR = SNR\sqrt{N}$ (minimum expected improvement)

where

N = Number of pulses integrated

2.2.2 Modulated Retroreflector

This concept employs a wind driven modulated retroreflector assembly mounted on the landing gear strut and arresting hook as shown in Figure 2-1. The speed of rotation is controlled by blade and bearing design. Modulation is determined by the number and placement of retroreflectors within the assembly and by the number and width of blades. In the example above, the primary retroreflector (strut mounted) is used to provide aircraft identification. The secondary modulation frequency is generated by the tailhook assembly. Indication of the gear down and hook down are given by the presence of both frequencies in the signal return. This concept uses a CW CO_2 sealed waveguide laser and a HgCdTe cooled detector system with nominal systems parameters as shown in Table I. The choices represent components well within the current state of the art.

A signal-to-noise ratio analysis was conducted with the listed parameters. The results are shown in Figure 2-2. Detailed inspection of the results shows that the SNR is dominated by laser effects for the shorter ranges including laser amplitude fluctuation, speckle noise and target cross section variations. At longer ranges turbulence induced scintillation dominates the results. This analysis shows that increases in turbulence levels in general have a dramatic effect on SNR; however, Figure 2-3 indicates that turbulence levels over the ocean may rarely be expected to exceed $C_n^2 = 1.0 \times 10^{-15}\ m^{-2/3}$. Thus the SNRs are more than adequate for ranges out to five kilometers.

We conclude that in clear weather, the modulated retro-reflector concept affords acceptable performance; however, the maximum information content is limited to gear status, hook status aircraft type, or similar data.

2.2.3 Uni-directional Optical Data Link

This concept employs a one-way optical communications data link from air to ship as shown in Figure 2-4. A strut mounted laser diode transmitter is mounted on the landing gear of the aircraft and PCM-modulated to downlink aircraft type, tail number, hook down, gear down, fuel state and an optional one way voice channel. The transmitter uses no optics and begins operation automatically as the landing gear is extended. Current laser diode technology supports pulse rates in excess of 10 khz assuring overall update rates of 1 per second or less 8

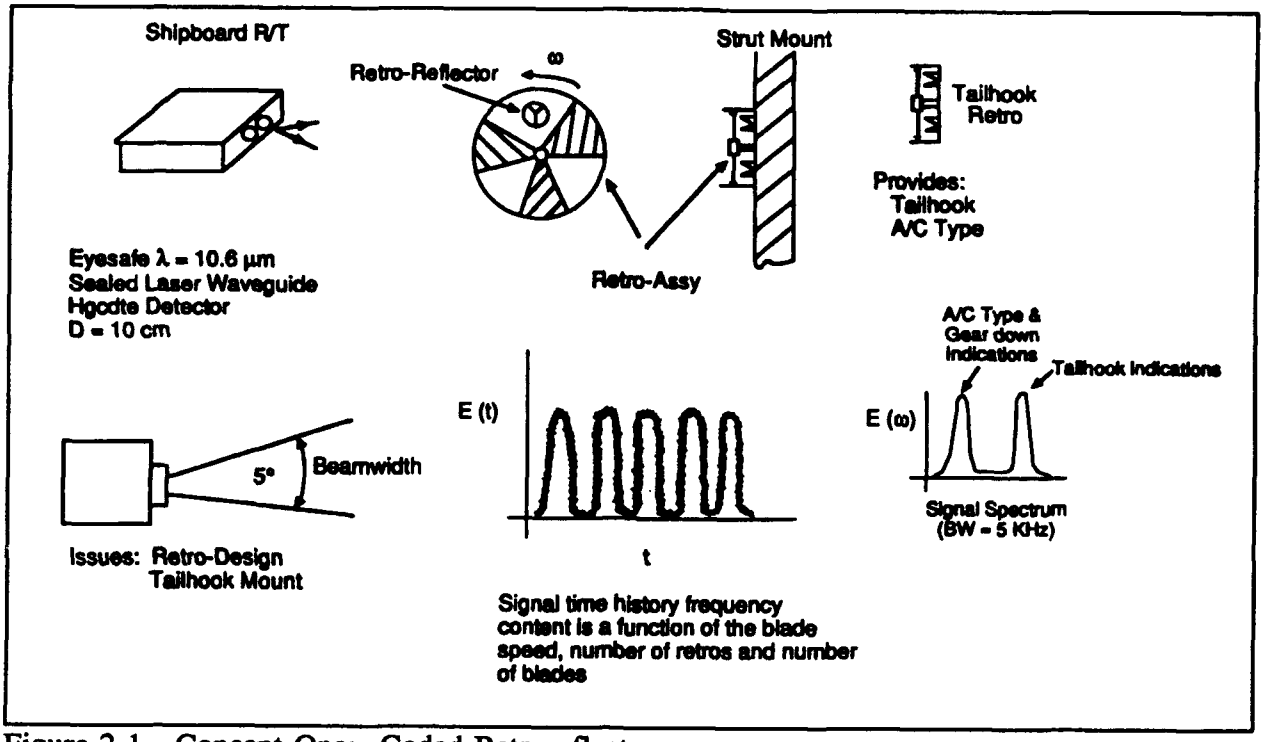

Figure 2-1. Concept One: Coded Retroreflector

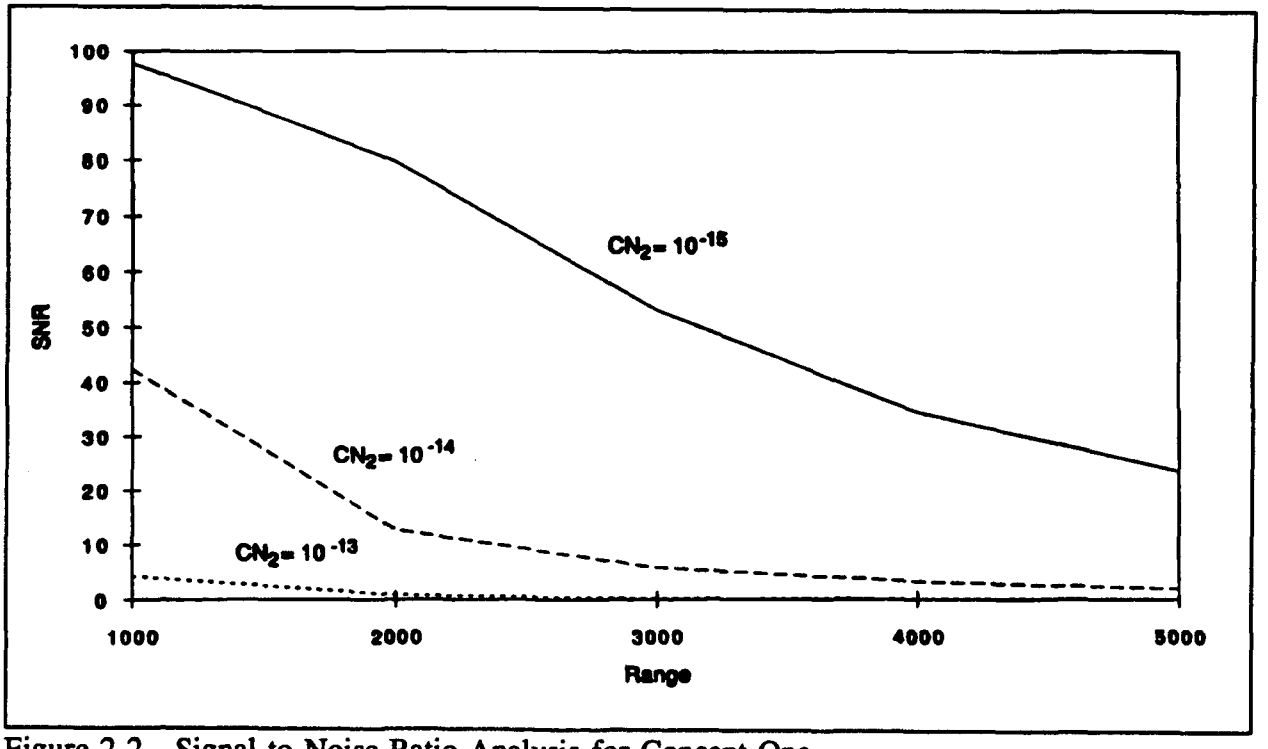

Figure 2-2. Signal-to-Noise Ratio Analysis for Concept One

Table I Modulated Reflector Input Parameters		
Parameter	Value	Units
Laser Power	100	w (cw)
Laser Pulse Length	N/A	
Target Cross-Section	1.0×10^{6}	m^2
Receiver Diameter	.1	m
Absorption	.279	km-1
Initial Range	1000	m
Optical Efficiency	.8	
Noise Factor	2	
Background Spectral Radiance	1.5E-10	w cm^{-2} sr^{-1} μm^{-1}
Responsivity	7.1	amp w^{-1}
Temperature	N/A	
Receiver Gain	1	
System FOV	.1	rad
Dark Current	7.9E-10	Amp
System Bandwidth	5000	Hz
Load Resistor	50	ohn
Wavelength	10.6	μm
Number of Pulses Interated	1	
Cn2	1E-15	
Elec. Eff.	.6	
$\alpha^{2cs} = .1$, $\alpha^{2s} = .1$, $\alpha_2 1 = .02$		
Backscatter Coef	1.0×10^{-7}	
Preamp RMS Noise Current	4.45E-09	amp

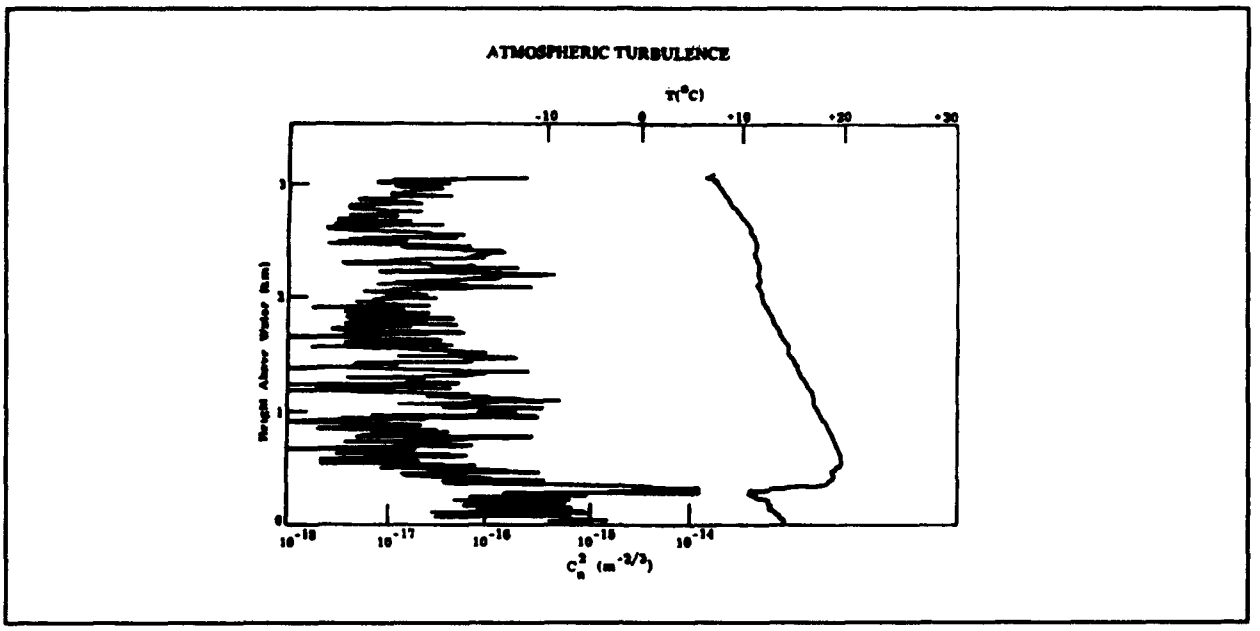

Figure 2-3. Typical Oceanic Turbulence Levels

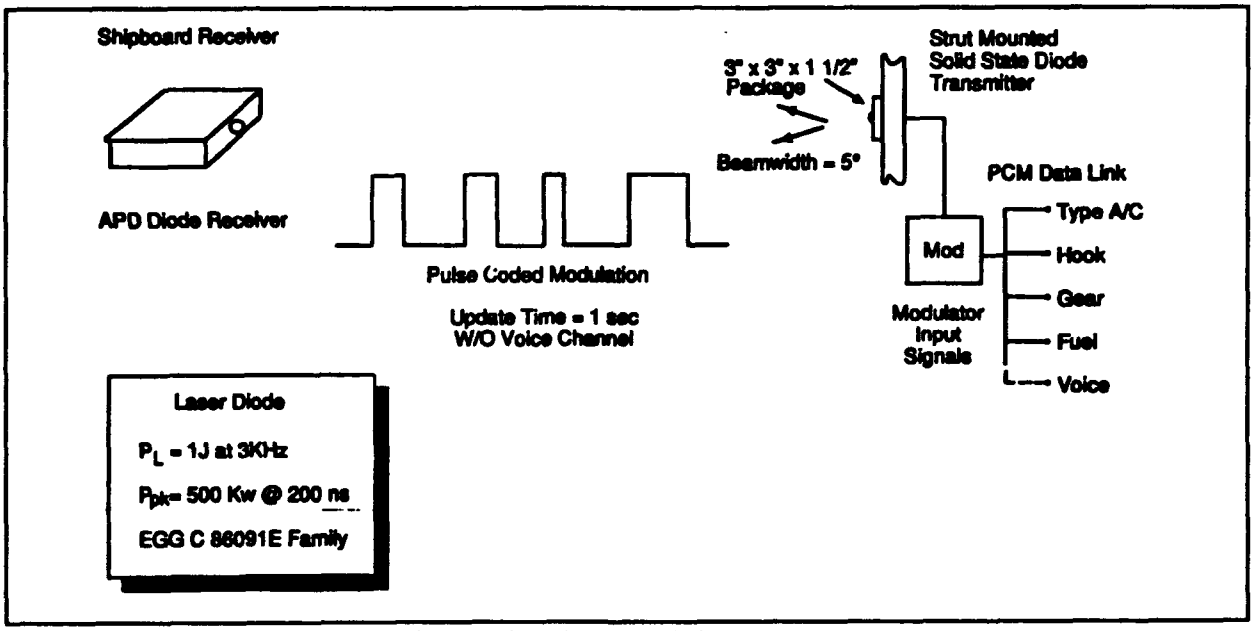

Figure 2-4. Concept Two: Uni-directional Data Link

without the voice channel. The shipboard receiver uses an off-the-shelf avalanche photodiode with systems parameters as shown below in Table II. The results of the signal to noise analysis are shown in Figure 2-5. For benign turbulence level the SNR performance is acceptable at ranges out to five kilometers degrading rapidly as the turbulence strength increases. Overall performance at the shorter wavelengths is turbulence limited.

We conclude that the performance of the uni-directional optical data link in clear weather is acceptable over the ranges of interest and for benign turbulence levels as expected over the ocean. The information content of this link is substantial with a modest increase in cost and complexity over the modulated retro-reflector concept.

2.2.4 Bi-directional Optical Communications Link

This concept as shown in Figure 2-6 is a two-way optical voice link with data channels as in the previous case. The principal difference is the addition of an optical receiver to the aircraft and a laser transmitter to the ship installation markedly increasing the cost and complexity of both. Because of size constraints, aircraft receiver optics are limited to relatively small apertures. The gain in performance of this configuration is in the addition of the ship-to-aircraft voice link. This would allow LSO communications during the approach, at the cost of some complexity. The input parameters for this configuration are shown in Table III. They are similar to the one way link. Performance of this configuration is limited by the aircraft receiver and is shown in Figure 2-7. The SNRs are again turbulence limited; however, acceptable performance is achieved for most of the operating envelope. Again performance degrades rapidly for increased levels of turbulence due to the relatively short wavelengths and the modest size of the receiver aperture on the aircraft.

2.2.5 SNR Performance Summary

The SNR performance is shown for a relatively narrow range of possible input conditions. This is particularly true of certain input parameters such as the laser power. Since the performance is largely turbulence-limited, the lower limits of laser output power have not been

Table II Uni-directional Data Link Input Parameters		
Parameter	Value	Unit
Laser Power	500000	w
Laser Pulse Length	2.0×10^{-7}	
Target Cross-Section	N/A	
Receiver Diameter	.1	m
Absorption	.055	km-1
Initial Range	1000	m
Optical Efficiency	.8	
Noise Factor	2	
Background Spectral Radiance	1.5E-10	w cm^{-2} sr^{-1} μm^{-1}
Responsivity	.93	
Temperature	N/A	
Receiver Gain	10	
System FOV	.1	rad
Dark Current	3.47E-10	amp
System Bandwidth	10000	Hz
Load Resistor	N/A	
Wavelength	1.54	μm
Number of Pulses Integrated	10	
cn^2	1E-15	
Elec. eff.	.8	
Sigma cs	.1 sigma speckle = .1 sigma laser = .05	
Backscatter Coef	1.0×10^{-6}	
Preamp rms Noise current	1.35E-08	amp

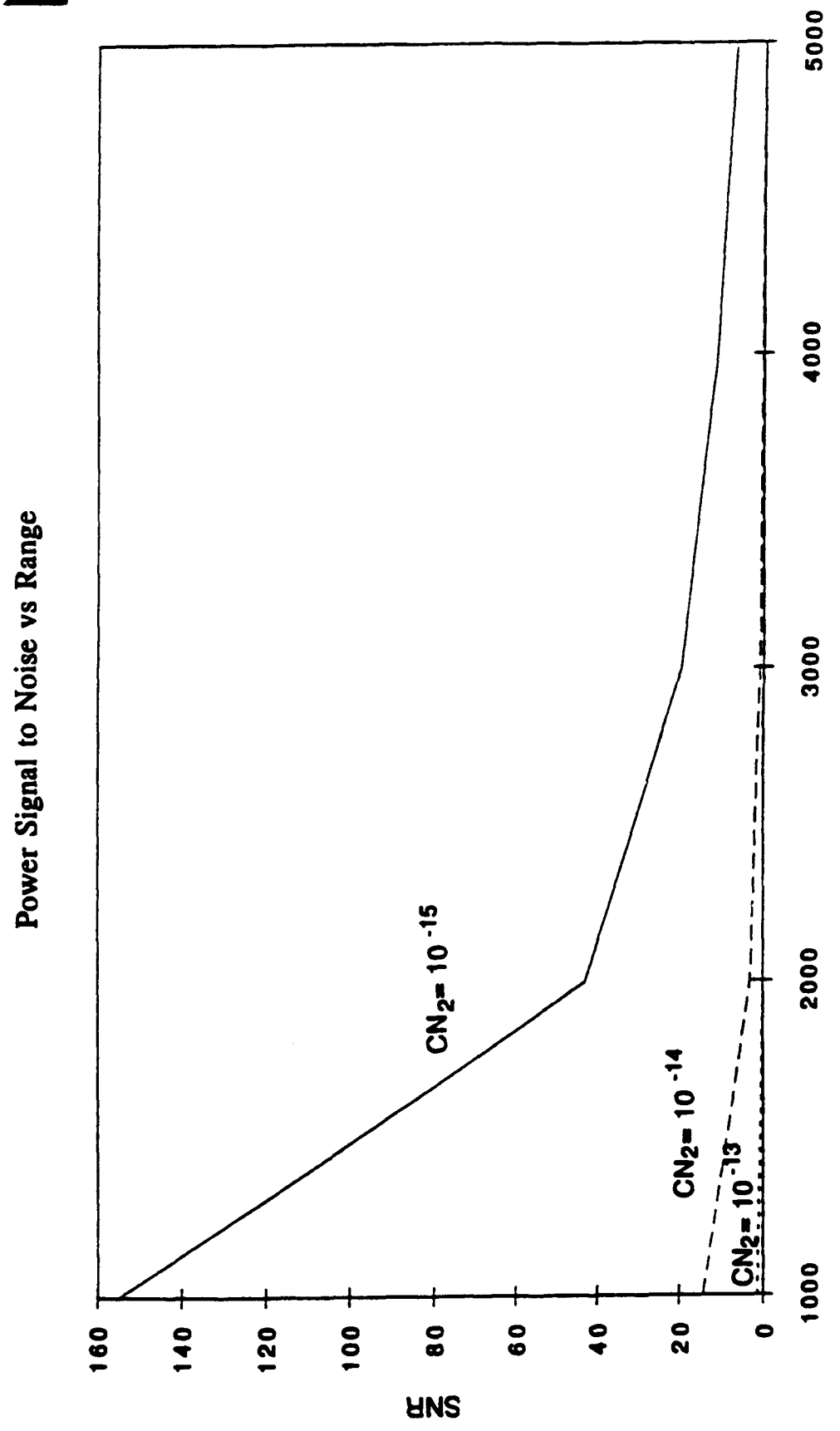

Figure 2-5. Uni-directional Data Link

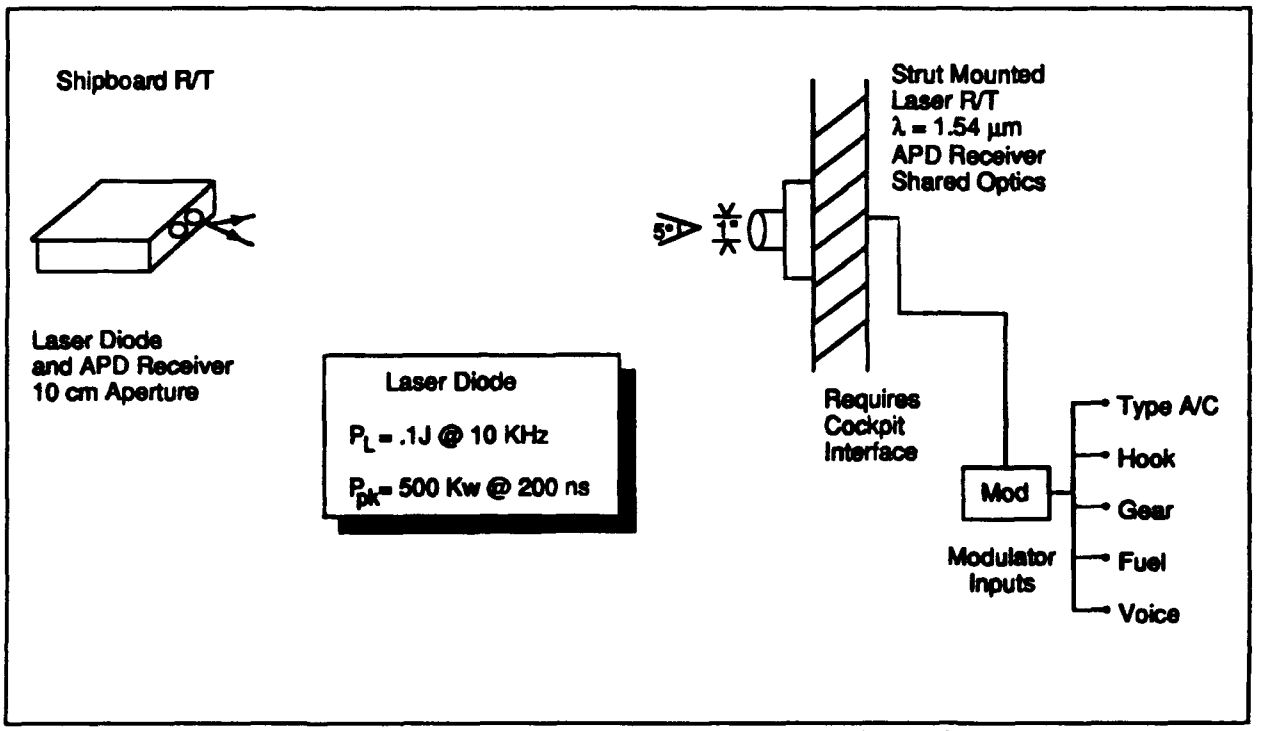

Figure 2-6. Concept Three: Bi-directional Optical Communications Link

Table III Bi-directional Data Link Input Parameters		
Laser Power	500000	w pk
Laser Pulse Length	2.0×10^{-7}	
Target Cross-Section	N/A	
Receiver Diameter	.025	m
Absorption	.055	km-1
Initial Range	1000	m
Optical Efficiency	.8	
Noise Factor	2	
Background Spectral Radiance	2.5E-08	w cm^{-2} sr^{-1} μm^{-1}
Responsivity	.93	
Temperature	N/A	
Receiver Gain	10	
System FOV	.1	rad
Dark Current	3.47E-10	amp
System Bandwidth	10000	Hz
Load Resistor	50	ohm
Wavelength	1.54	μm
Number of Pulses Integrated	1	
cn2	1E-15	
Elec. Eff.	.8	
Sigma cs	N/A sigma speckle N/A sigma laser = .05	
Backscatter Coef.	1.0×10^{-6}	
Preamp RMS Noise Current	1.35E-08	amp

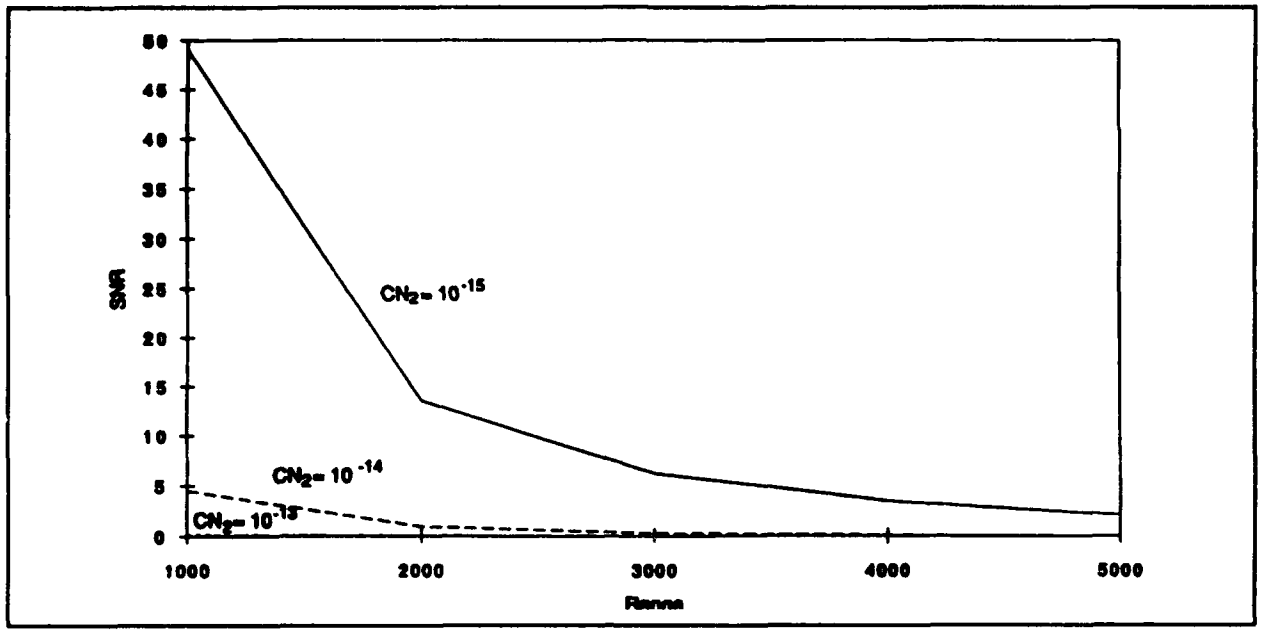

Figure 2-7. SNR for Bi-directional Data Link

fully explored and it is likely that much less laser output power will be required in all of the above configurations. This will relax eye safety concerns potentially reducing the output power well below the eyesafe threshold, which in turn may admit the use of GaAs or other well developed technology.

A relative cost performance matrix is shown in Table IV. As expected cost/complexity is proportional to information content. The only modest development risk anticipated is the retro-assembly design. Constancy of rotational speed is a crucial issue as is the feasibility of mounting the assembly on an aircraft tailhook.

2.2.6 Modulation and Performance of Direct-Detection Optical Communication Links

The modulation schemes most often used in direct detection optical communication systems include pulse-gated binary modulations (PGBM) and pulse-position modulation (PPM). In PGBM the binary data are transmitted as a sequence of optical pulses, such that a binary "one" is transmitted by the presence of a pulse, while the absence of a pulse denotes a binary "zero." Alternately, information can be encoded in the PPM scheme. In an M-ary PPM system each word frame is divided into M slots. Information is then transmitted by sending an optical pulse

Table IV

Concept Relative Merit Matrix

Concept	Performance	Risk	Cost	Info. Content
Modulated Retro	highest	Medium	Low	Low
Uni-directional Data Link	Medium	Low	Medium	Medium
Bi-directional Communications Link	Lowest	Low	High	High

in one of the M slots. Photons are counted in each slot and a pulse is declared to be in the slot with the highest count. Figures 2-8 and Figure 2-9 exemplify both encoding schemes. PPM enjoys two significant advantages over PGBM. First, multiple bits of information can be transmitted using a single pulse, hence PPM is more power efficient than PGBM. Second, PPM can be decoded regardless of the signal and background strength, unlike PGBM where the optimum decision threshold is dependent on the signal and background levels. Because of these advantages PPM is the preferred modulation and this discussion will focus on PPM as the modulation format.

The purpose of the digital demodulator (for the case of an M-ary system) is to determine which of the M waveforms $\{S_k(t)\}$ was transmitted, given the detector output r(t). In order to decode the transmitted information, the receiver performs the maximum a posteriori (MAP) decision. Under this criterion, the output of the photodetector is observed over a given symbol period $(0, MT_s)$. The decoder then selects the codeword that has the highest probability of having been transmitted. Mathematically, given the output of the photodetector r(t), $0 \leq t \leq MT_s$, the decoder selects the codeword which maximizes $P(S_k(t)/r(t))$, the probability that $S_k(t)$ was transmitted, given the received signal is r(t). For an M-ary block-encoded system, the decoder outputs the k^{th} codeword if $P(S_k(t)/r(t))$ is the largest among the M a posteriori probabilities.

In general, this probability is difficult to calculate. Usual assumptions made in system evaluation ignore the effects of thermal noise and detector gain noise. However, in the direct-detection ISL most likely the gain of an avalanche photodiode (APD) must be utilized due to the rather low signal levels detected at the receiving antenna. In this case the effects of detector gain noise cannot be ignored.

Figure 2-10 shows a typical PPM demodulator. The detailed statistics of the APD output are difficult to characterize. However, for communication receivers, the outputs of each of the M integrators can be effectively approximated using Gaussian statistics. Specifically, the mean and the variance of the k^{th} integrator output can be written as

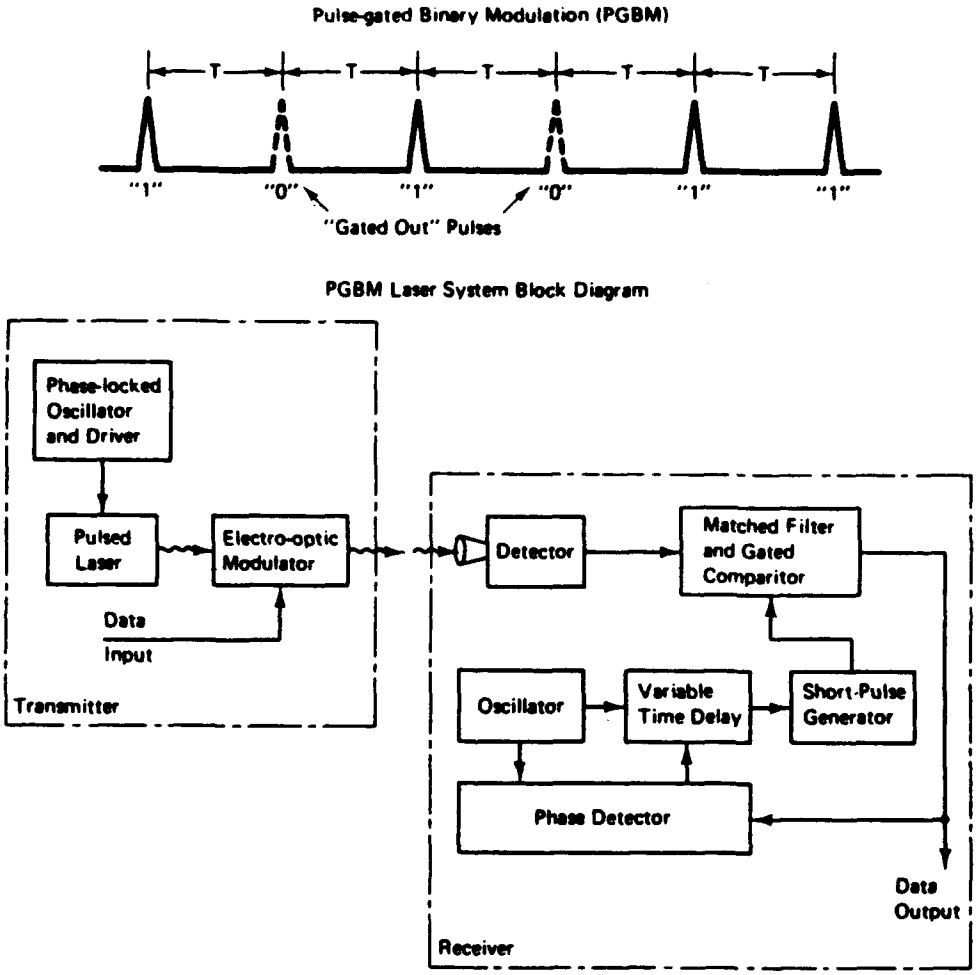

Figure 2-8. Pulse-Gated Binary Modulation (PGBM). Information is conveyed by the presence or absence of an optical signal in bit period T. Since no signal is transmitted for a "0", the signal-to-noise ratio for 1 and 0 are not symmetric.

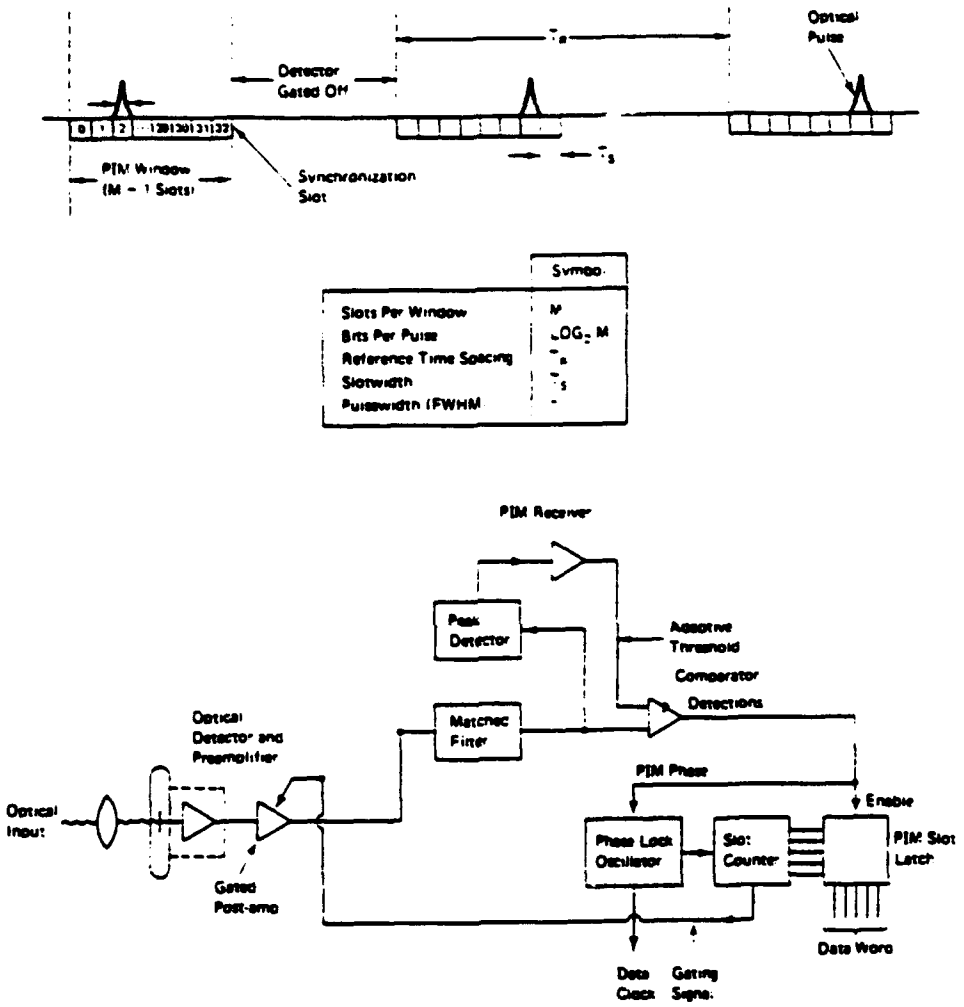

Figure 2-9. Pulse Interval Modulation (PIM) Formation and Receiver. Two options exist for PIM. Data can be transmitted by modulating the time interval between two pulses or by modulating the transmission time of a signal pulse with respect to a fixed reference.

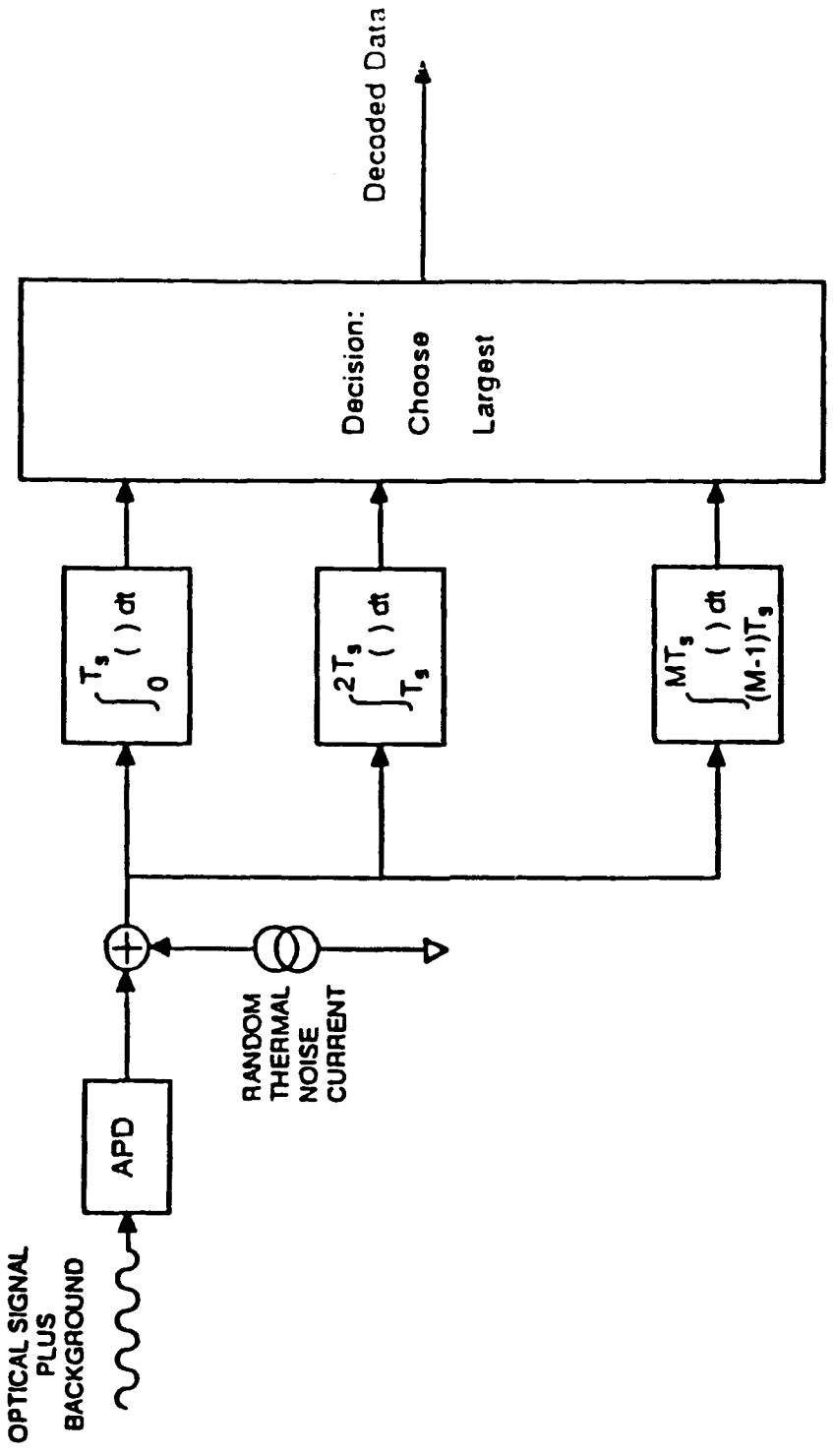

Figure 2-10. Model of a PPM Demodulator

$$E[X] = G\left[K_s + K_B + \frac{I_b T_s}{e}\right] + \frac{I_s T_s}{e} \cdot$$

$$var[X] = G^2 F\left[K_s + K_B + \frac{I_b T_s}{e}\right] + \frac{I_s T_s}{e} + K_{Th}^2$$

where $x = \frac{1}{e}\int_o^{T_s} i(t)\,dt$ is the integrator output

$i(t)$ = APD Current

I_b = Gain Dependent Dark Current

I_s = Gain Independent Dark Current

K_{Th}^2 = Thermal Noise Variance

G = APD Gain

F = APD Excess Noise Factor

K_s = Signal Photocount

K_B = Background Photocount

Since only one time slot contains the signal pulse, the integrator outputs for the remaining (M-1) time slots are identically distributed. Consequently, the PWE (probability of word error) for the M-ary PPM channel can be written as

$$P_{WE} = 1 - \left\{\int_{-\infty}^{\infty} \frac{1}{\sqrt{2\pi}} e^{-(x-\mu_1)2/2\sigma_1^2} \int_{-\infty}^{x} \frac{1}{\sqrt{2\pi}\,\sigma_0} e^{-(y-m_0)2/2\sigma_0^2}\,dy^{M-1}\,dx\right\}$$

$$\text{where } \mu_0 = \left[K_B + \frac{I_b T_s}{e} \right] + \frac{I_S T_S}{e}$$

$$\mu_1 = G \left[K_s + K_B + \frac{I_b T_s}{e} \right] + \frac{I_s T_s}{e}$$

$$\sigma_0^2 = G^2 F \left[K_B + \frac{I_b T_s}{e} \right] + \frac{I_s T_s}{e} + K_{Th}^2$$

$$\sigma_1^2 = G^2 F \left[K_s + K_B + \frac{I_b T_s}{e} \right] + \frac{I_s T_s}{e} + K_{Th}^2$$

The signal-to-noise ratio (SNR) of the APD-based PPM receiver can be defined as

$$p = \frac{(\mu_1 - \mu_0)^2}{\sigma_1^2 + \sigma_0^2} = \frac{G^2 K_s^2}{G^2 F \left[K_s + 2K_B + 2 \frac{I_b T_s}{e} 75 \right] + 2 \frac{I_s T_s}{e} + 2K_{Th}^2}$$

The gain of the APD is an important parameter which must be specified. The higher the detector gain, the smaller the effect of thermal noise on the receiver SNR. However, higher detector gain also implies a larger excess noise factor for the APD, which in turn can reduce the receiver SNR. Consequently, given the receiver parameters and the signal and background power, there is an optimum detector gain which maximizes the SNR.

Another factor to consider in the channel is the presence of a finite extinction ratio. The extinction ratio, m, is defined as the ratio of the source output power when in an "off" (binary 0) state to that when in an "on" (binary 1) state. The signal and background photocounts can be related to the average signal and background power by

$$K_s = \frac{\alpha P_s T_w}{1 + m(M-1)}$$

$$K_B = mK_s + \alpha P_B T_s$$

where m = Extinction Ratio
M = The PPM Order
α = Detector Responsivity

T_w = Word Period ($\log^2$ M/R)
R = Data Rate
P_s = Signal Power
P_B = Background Power

The receiver SNR can then be written as a function of the signal and background power, as well as the data rate:

$$p = \frac{G^2\alpha^2 P_s^2 M \log_2(M)/R\,[1 + m(M-1)]^2}{G^2F\left[(1+2m)\frac{\alpha P_s M}{1+m(M-1)} + 2\alpha P_B + \frac{2I_b}{e}\right] + \frac{2I_s}{e} + 2\frac{2K_B\,Teq}{R_L\,e^2}}$$

In the presence of a finite extinction ratio, m, the receiver SNR first increases with increasing M until an optimum SNR is reached, and further increases in M only result in a smaller SNR. It should be noted that in the derivation of this equation it was assumed that the average power was maintained at a constant level regardless of the PPM order. This implies that the peak transmitter power increases linearly with M. In practice this poses a limitation on the resulting PPM order achieved and the optimum order is determined by the ratio of peak power to average power as well as the extinction ratio m. This results in an optimum value of $M \simeq 10$ for extinction ratios between 1% and 10%. A value of $M = 10$ will be assumed in the remainder of this analysis.

The Probability of Bit Error (PBE) is related to P_{WE} (p. 18) by the expression

$$P_{BE} = \frac{2^{n-1}}{2^n-1} P_{WE}$$

where

$$n = \log_2 M$$

Using this expression we can relate the power SNR at the receiver to the PBE, as is shown in Figure 2-11. It should be noted that the above results for receiver performance were derived ignoring the effects of spatial and temporal tracking errors. In the presence of such errors

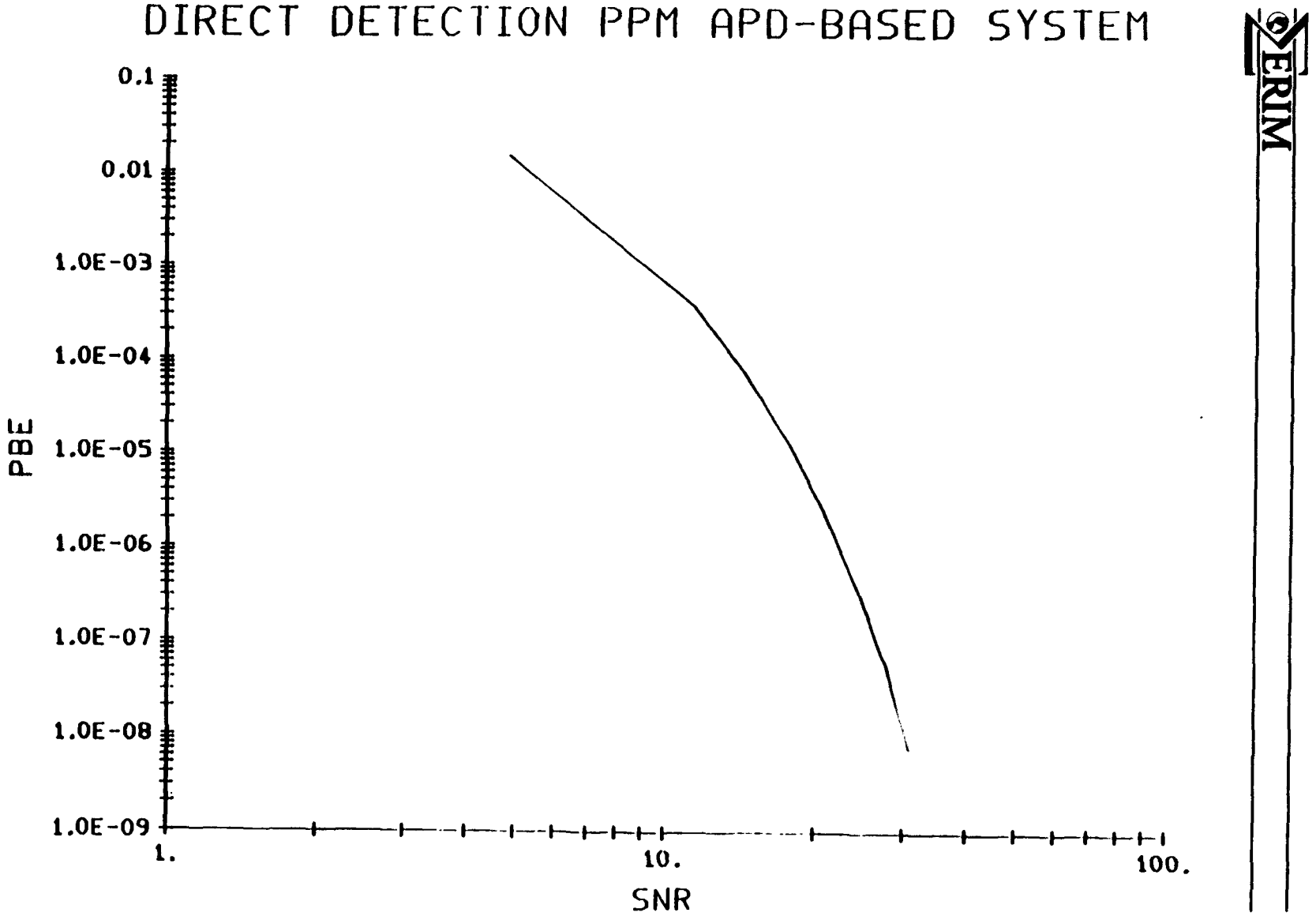

Figure 2-11. PBE vs. SNR at the Receivers

performance will degrade somewhat from that given. The overall system design must be optimized taking into account the achievable tracking error. For direct detection systems this optimization takes the form of tailoring the transmitter beamwidth to minimize the required source power for a given error rate.

The signal count collected at the direct detection receiver is a function of the transmitter power P_L, the transmitter antenna gain G_T, and the instantaneous pointing error θ_T. For an M-ary PPM system operating at wavelength λ over a range of Z meters, the signal count K_s can be taken as

$$K_s(P_L, G_T, \theta_T) + \eta_T G_T \left[\frac{\lambda}{r\pi z}\right]^2 \eta_R G_R L_T(G_T, \theta_T) M \left[\frac{\eta}{h\nu}\right] P_L T_s$$

where

η_T = Efficiency of transmitting optics

η_R = Efficiency of receiving optics

G_T = Transmitter antenna gain

G_R = Receiver antenna gain

P_L = Average transmitter power

T_s = Time per PPM subslot period

L_T = Pointing loss factor associated with instantaneous pointing error θ_T.

This equation assumes that the peak transmitter power is M times the average power. The receiver antenna gain G_R, transmitter antenna gain G_T, and pointing loss factor (assuming a uniformly illuminated transmit aperture) $L(G_T, \theta_T)$ are given by

$$G_R = \left[\frac{\phi d_R}{\lambda}\right]^2$$

$$G_T = \left[\frac{\phi d_T}{\lambda}\right]^2$$

$$L_T(G_T, \theta_T) = \left[\frac{2\, J_1(\phi \theta_T \partial_T/\lambda)}{\phi \theta_T \partial_T/\lambda}\right]^2 = \left[\frac{2\, J_1\left(\sqrt{G_T}\ \theta_T\right)}{\sqrt{G_T}\ \theta_T}\right]^2$$

where

d_T = Transmit antenna diameter

d_R = Receive antenna diameter

2.3 SUMMARY AND CONCLUSION

The three concepts examined show acceptable performance within the validity of the assumed operation parameters. The signal to noise ratios are driven strongly by turbulence levels in all cases. Nevertheless, expected turbulence values over the ocean do not result in unacceptable performance. We have shown that for the assumed modulation format, the probability of word error is acceptable for the expected SNR ratios. We conclude that implementation of any of the concepts considered herein is well within the bounds of feasibility with currently available electro-optical components. The final choice is a matter of information content versus cost.

3.0 TASK 6: RESEARCH ON TRACKING AIRCRAFT USING SPREAD SPECTRUM TECHNOLOGY

The objective of this task is to assess various approaches for aircraft tracking based on spread spectrum technology. Spread spectrum technology is being considered as a means of reducing the probability of intercept of active tracking systems. When the probability of intercept is sufficiently low, use of active tracking systems can be considered during emissions control (EMCON). The operational scenario that will be addressed in this study is the intermediate tracking (approximately ten nautical miles) stage. Two specific transmit receive architectures are also examined: 1) beacon on aircraft; and 2) spread spectrum waveform from a range/doppler radar on board ship. During the study, we examined the required signal bandwidths such that the tracking signal is at ambient levels at ten nautical miles and the amount of beam spreading due to the large bandwidth for a fixed antenna size.

3.1 SPREAD SPECTRUM BACKGROUND

Spread spectrum technology has become critically important in many areas including communication, tracking, and radar. A good review of spread spectrum technology is contained in [3.1]. Spread spectrum technology is based, as its name implies, on expanding or spreading the bandwidth of a signal. The spreading of the bandwidth is accomplished via many encoding methods; the two most common spread spectrum signals are direct sequence and frequency hopped. By spreading the spectrum and modulating the signal with a unique code a number of very favorable benefits ensue: 1) many data links can exist on the same frequency band; 2) LPI/LPE threat is significantly reduced; and 3) improved range Doppler performance can be obtained in a system.

The very common type of spreading code is the linear code. This type of code is generated by a finite state machine whose architecture is known to both the transmitter and receiver. An example of such a machine is shown in Figure 3-1. To generate a direct sequence signal, this code can be added modulo 2 to the binary signal traffic. The period of the spreading code is some multiple N smaller than the period of the signal traffic. The inverse of the period of the spreading code is called the chip rate of the code. The ratio of the period of the signal traffic to the spreading code is the amount of bandwidth spreading the modulation provides. Finally,

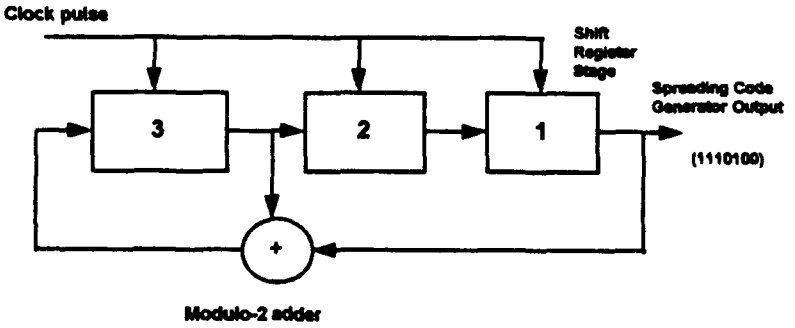

Figure 3-1. Block Diagram of a Shift Register Generator

the spread signal is modulated and sent down the communication channel. The type of modulation can be phase or frequency shift keying, etc. A block diagram depicting the functions of a spread spectrum transmitter is shown in Figure 3-2.

Spread spectrum receivers are required to perform a number of functions. In a cooperative environment, the receiver has an exact replica of the spreading code generator and must only time synchronize and demodulate the transmitted traffic. Time synchronization is done by a correlation operation. When the receiver is time aligned to the incoming traffic, the signal is despread via a modulo 2 addition between the incoming signal and the spreading code. This is the analogous operation to the transmitter. The despread traffic is then demodulated from the specific modulation method used. Figure 3-3 shows an example of the receiver operations in a cooperative environment. Figure 3-4 shows the effect of the despreading operation on the traffic bandwidth. The spectral compression is equivalent to the amount of spreading at the transmitter.

Noncooperative receivers have a more arduous task. These receivers have no knowledge that there is traffic nor knowledge of the spreading code. These receivers must detect the presence of a spread spectrum signal (the interception problem), identify the center frequency of modulation and the chip rate (feature extraction), and estimate the machine which generates the spreading code. In addition, the receiver must become time aligned such that despreading can occur. These tasks have been the subject of intensive research and will not be reviewed in total here. Our consideration is only the intercept problem. In this problem, an intercept receiver is interested in detecting the presence of a transmitter (spread spectrum or otherwise), determining its direction and estimating a few of its parameters. The classical architecture of intercept receivers is the radiometer. The radiometer receiver gathers energy in a specific band. If the amount of collected energy exceeds a threshold, a detection occurs. This will be the basis of our analysis.

3.1.1 System Analysis

The first scenario which will be examined is the use of a beacon on the airplane. Tracking of aircraft systems often use UHF (700 MHz) systems. To maintain a one meter range resolution, a bandwidth of 150 MHz must be used. The 20% bandwidth rule of thumb for

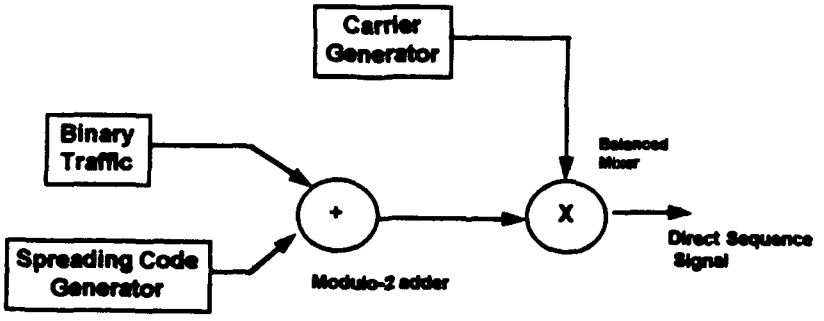

Figure 3-2. Block Diagram of a Direct Sequence Signal Transmitter Using a Modulo-2 Adder

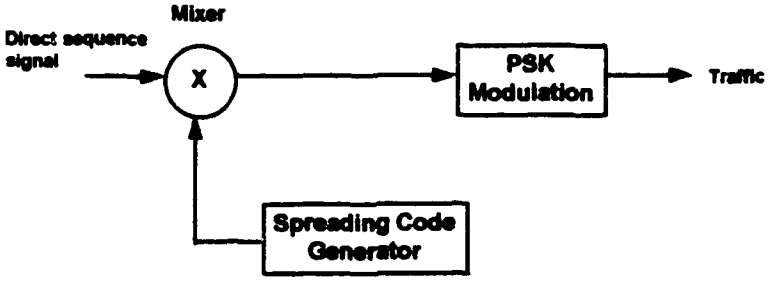

Figure 3-3. Receiver for a Modulo-2 Encoded Direct Sequence System

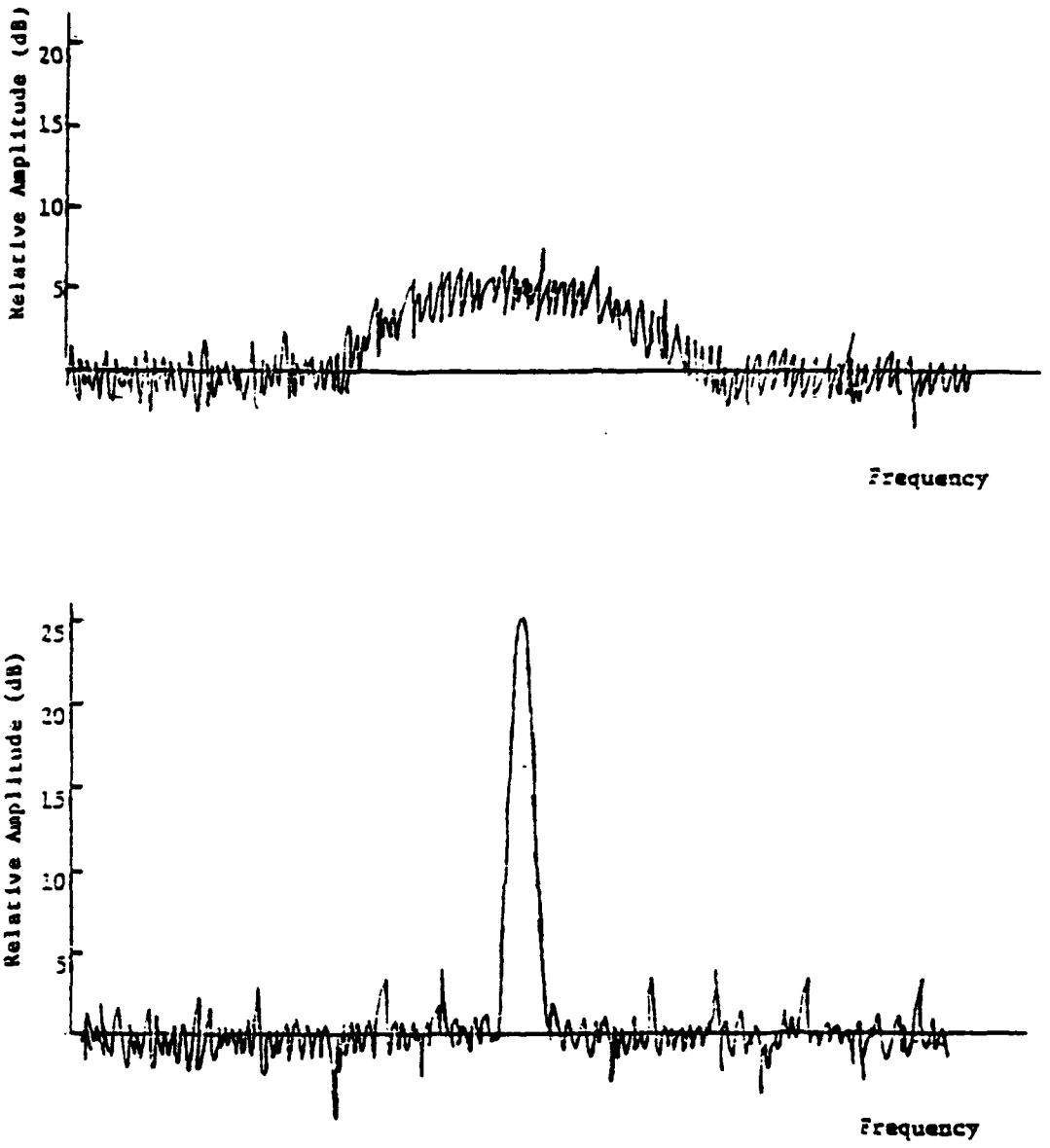

Figure 3-4. Frequency Spectrum of a Direct Sequence Signal and of a Decoded Receiver Output

systems provides approximately 140 MHz which would immediately be violated when any bandwidth spreading would be done. In addition, a spreading factor of five can only be accommodated before the entire spectrum at that center frequency is used. Consequently, it does not appear feasible that spread spectrum techniques would be useful in this scenario.

For the second scenario, the transmitter on the ship, the fundamental question to be answered in this analysis is what amount of bandwidth spreading must be done such that at 10 nmi, the transmitted radar signal is at ambient (i.e. SNR=1). The traffic bandwidth will be maintained at 150 MHz such that a 1 m range resolution of the radar is maintained. In order to proceed with this analysis the radar range equation (one way) determining the power at the receiver P_{REC} must be stated [3.2,3.3]

$$P_{REC}=\frac{P_T G_{TR} G_{RT} \lambda^2}{(4\pi)^2 R^2}$$

where P_T is the transmitter average power, G_{TR} and G_{RT} are the transmitter and receiver antenna gains, λ is the wavelength and R is the range from transmitter to receiver. In this analysis, we will assume that the intercept receiver antenna is isotropic ($G_{RT}=1$). In addition, the intercept receiver will be assumed to have a B=150 MHz bandwidth and a noise figure of 10 dB, a conversion loss of 6 dB, and an IF amplifier noise figure of 4 dB. The equivalent noise power temperature of the intercept receiver is [3.4] T=46210 K. This equates to a noise power of 96×10^{-12} Watts.

For the transmitter, we will use the specifications outlined in [3.5]. The transmitter uses a four foot antenna and operates at X-band (λ=33mm), the antenna gain can be calculated by

$$G=\frac{(4\pi)A_e}{\lambda^2}$$

where A_e is the antenna aperture area. The antenna gain is $G_{TR}=14 \times 10^3$ (41dB). The peak power of the transmitter is 50 kWatts with a pulse length of .2 μsec. At R=10 nmi (18.24 km) the amount of power received (P_{ave}=20 Watts) is $P_{rec}=5.8 \times 10^{-9}$ Watts. Therefore, a bandwidth expansion of a factor of 60 must be made such that the transmitted signal is at ambient. This is equivalent to a 9 GHz, bandwidth signal which uses the entire available bandwidth for an X

band system. Assuming that the bandwidth is equally distributed about 9 GHz, the azimuth resolution would be degraded by a factor of 2 for the same size antenna.

The amount of bandwidth expansion can be mitigated by power management of the transmitting radar. To explore this we need to define the following scenario: the incoming airplanes to be tracked are equipped with a cooperative receiver to the transmitting radar. This cooperative receiver is a matched filter whose detection and false alarm performance can be analzed via [3.6]

$$\frac{P_{rec}T}{kTemp} = (\beta - \zeta)^2$$

where β = erfc $^{-1}$ (2 Pfa) and ζ = erfc^{-1} (2 Pd) and T is the transmitter pulse length (.2 μsec). In our analysis, we will set the detection threshold such that a probability of false alarm of 10^{-6} is obtained. We will assume that the cooperative receiver equivalent noise tempoerature is the same as that for the non-cooperative receiver. In addition, we will assume that the cooperative receiver has a 1 m antenna which provides a gain of G_{RT} = 39 dB. This provides 39 dB more receiver power for the cooperative reeiver than the non-cooperative receiver. For average transmitter powers greater thab .4mW, the probability of detection of the signal is 1. This is a factor of 50,000. The implication is that by power management, no spectrum spreading is required.

A more conservative approach to this analysis is to assume that the antenna for the cooperative receiver is also isotropic. The only gain that is afforded to the cooperative receiver is from the matched filter processor. Figure 3-5 shows the cooperative receiver performance as a function of average transmitter power. Average transmitter powers above .4 Watts provide Pd=1. This is a factor of 50 which also implies that power management mostly mitigates the need for expanding the spectrum. Scaling the average transmitter power to .4 Watts would then only require a bandwidth spreading factor of 1.2. The resultant signal bandwidth would be 180Mhz. This is a very reasonable figure.

The feasibility of power management over large power ranges can be questionable technically. Therefore, a tradeoff analysis which attempts to ascertain the amount of power management and bandwidth spreading is required. To produce this analysis a model for the

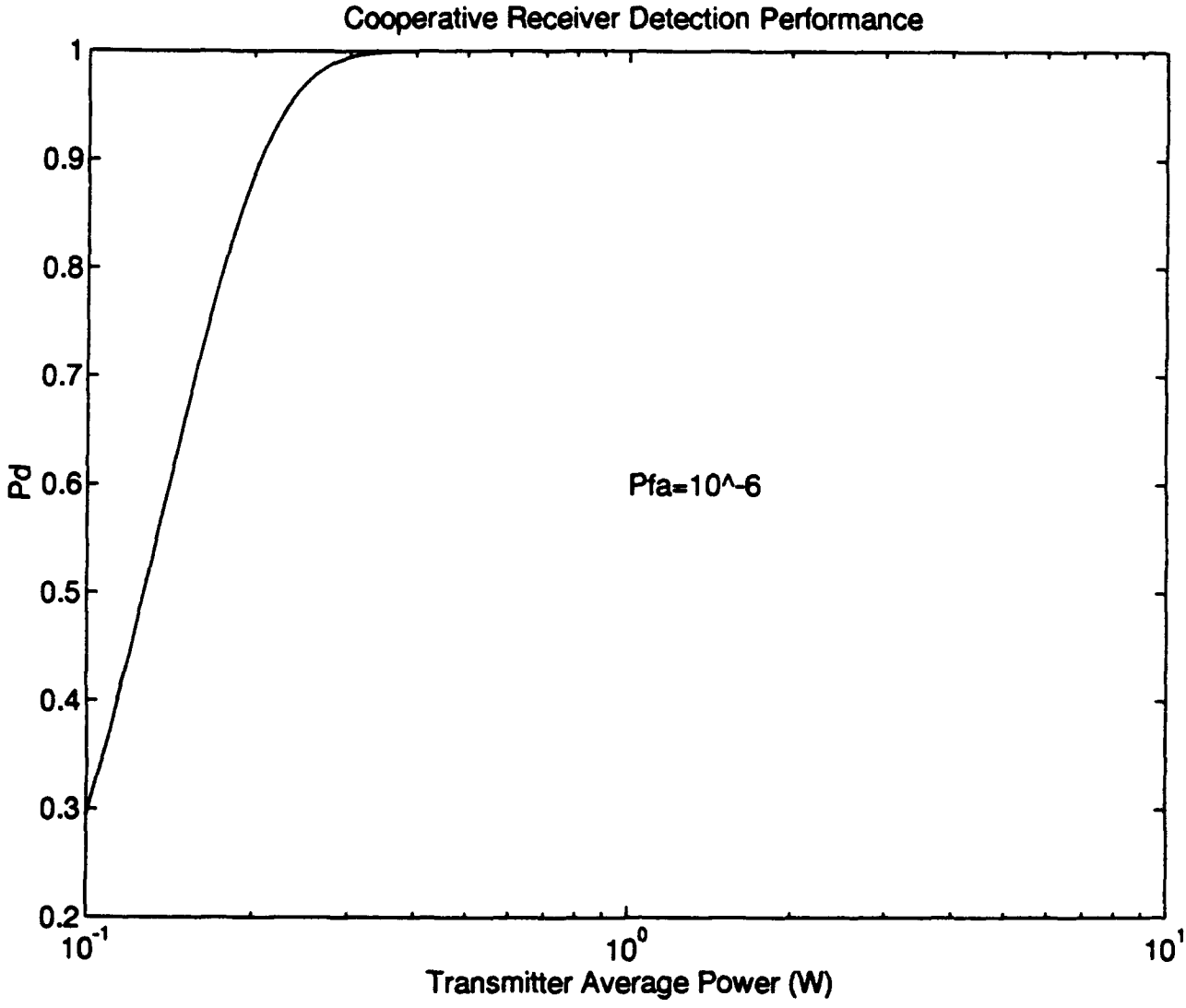

Figure 3-5. Cooperative Receiver Detection Performance vs. Transmitter Average Power (Isotropic Receiver Antenna)

intercept detection processor is needed. The intercept processor is a radiometer receiver which is characterized by

$$\frac{P_{rec}T}{kTemp} = (BW_{rec}t_{int})^{1/2}(\beta - \zeta)$$

where BW_{rec} is the non-cooperative receiver bandwidth (150 MHz) and T_{int} is the receiver integration time. The receiver integration time has a large bearing on the receiver performance. Figure 3-6 shows the intercept performance as a function of average transmitter power (signal bandwidth 300 MHz) when the receiver integration time is equal to the pulse length (.2 μs) or the pulse repetition period (500 μs). The simple power analysis implicitly assumes a radiometer matched to the pulse repetition period. Significantly better performance is attained when the receiver is integrating over the pulse time. This is due to the decrease in the amount of noise power integrated in the radiometer. Figure 3-6 shows that if the intercept receiver is assumed to be matched to the transmitter prf, the average transmitter power need only be reduced to 14 watts with a bandwidth of 300 MHz for a $P_{intercept} = .1$. Figure 3-7 shows the required average source power as a function of signal bandwidth for the non-cooperative receiver matched to the signal pulse repetition frequency for $P_{intercept} = .1$ and .01 and 2×10^{-6} (signal = ambient). This figure shows that for $P_{intercept} = .01$ and a signal bandwidth of 500 MHz, the average transmitter power need be 10 Watts. This is only a reduction by a factor of 2 in power. Figure 3-8 shows the required average source power as a function of signal bandwidth for the non-cooperative receiver matched to the signal pulse length for $P_{intercept} = .1$ and 01. These curves show a larger anount of required power reduction due to the better intercept performance of the receiver. These curves show that requiring the signal bandwidth be below 1 GHz implies that the average transmitter power must be below 1 Watt.

3.2 SUMMARY AND CONCLUSIONS

A cursory analysis of the applicability of spread spectrum techniques for LPI in a target tracking system has been performed. The initial result of the analysis shows that employing spread spectrum techniques in current systems without some sort of power management at the transmitter would not be feasible. By simultaneously managing power and spreading the signal

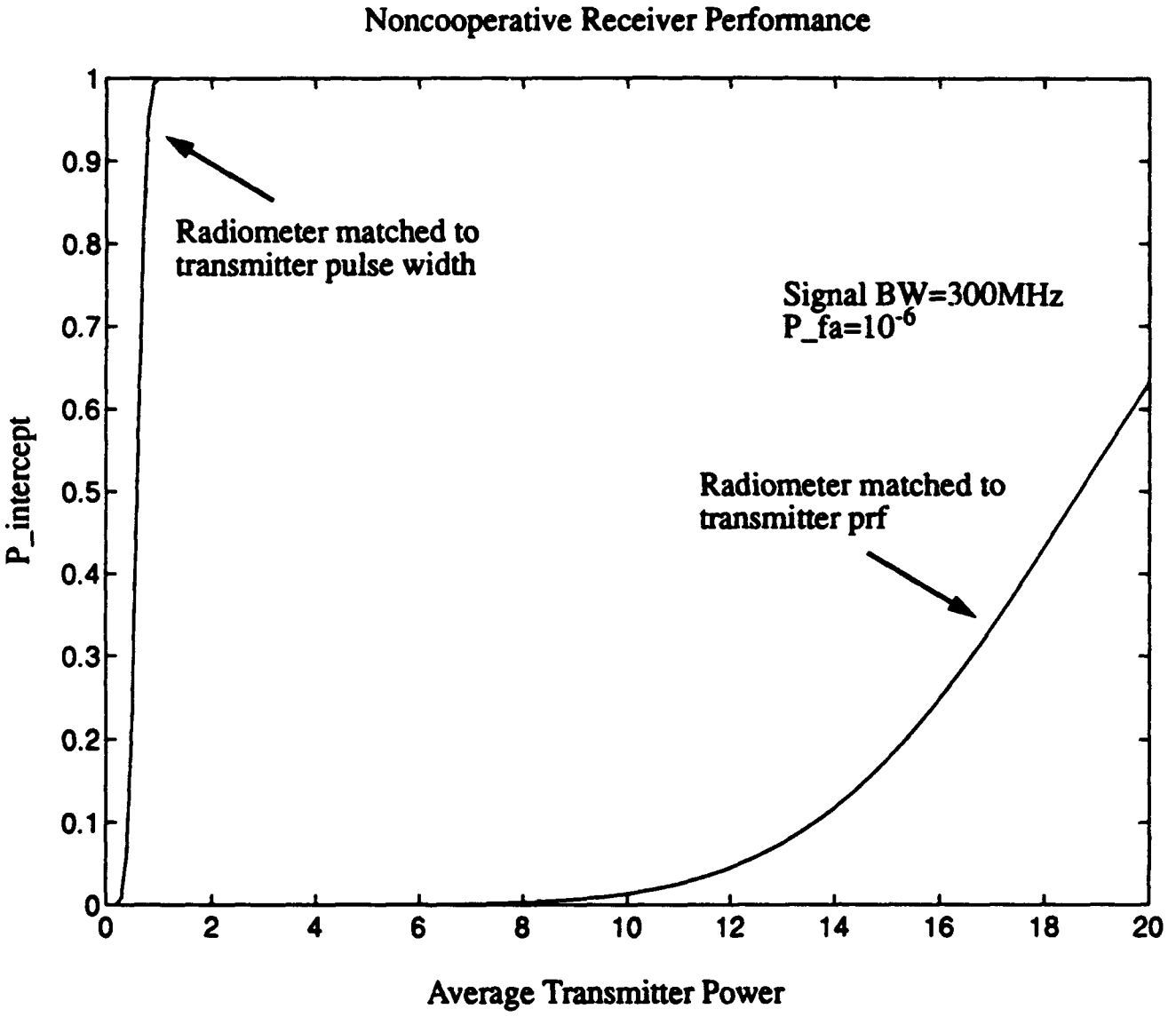

Figure 3-6. Non-cooperative Radiometer Receiver Performance vs. Transmitter Average Power

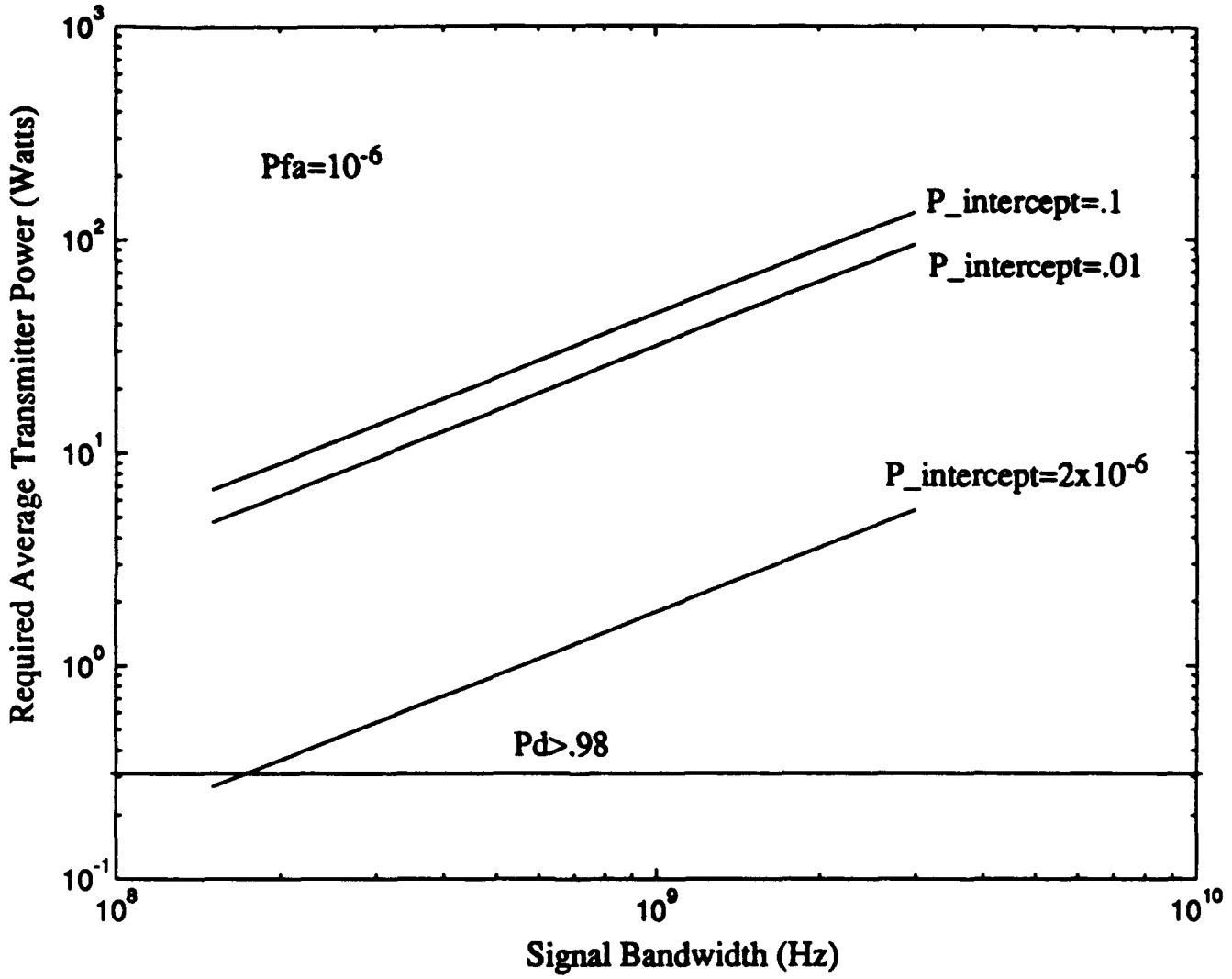

Figure 3-7. Average Power vs. Signal Bandwidth Trade-off for Radiometer Receiver Matched to Transmitter Performance

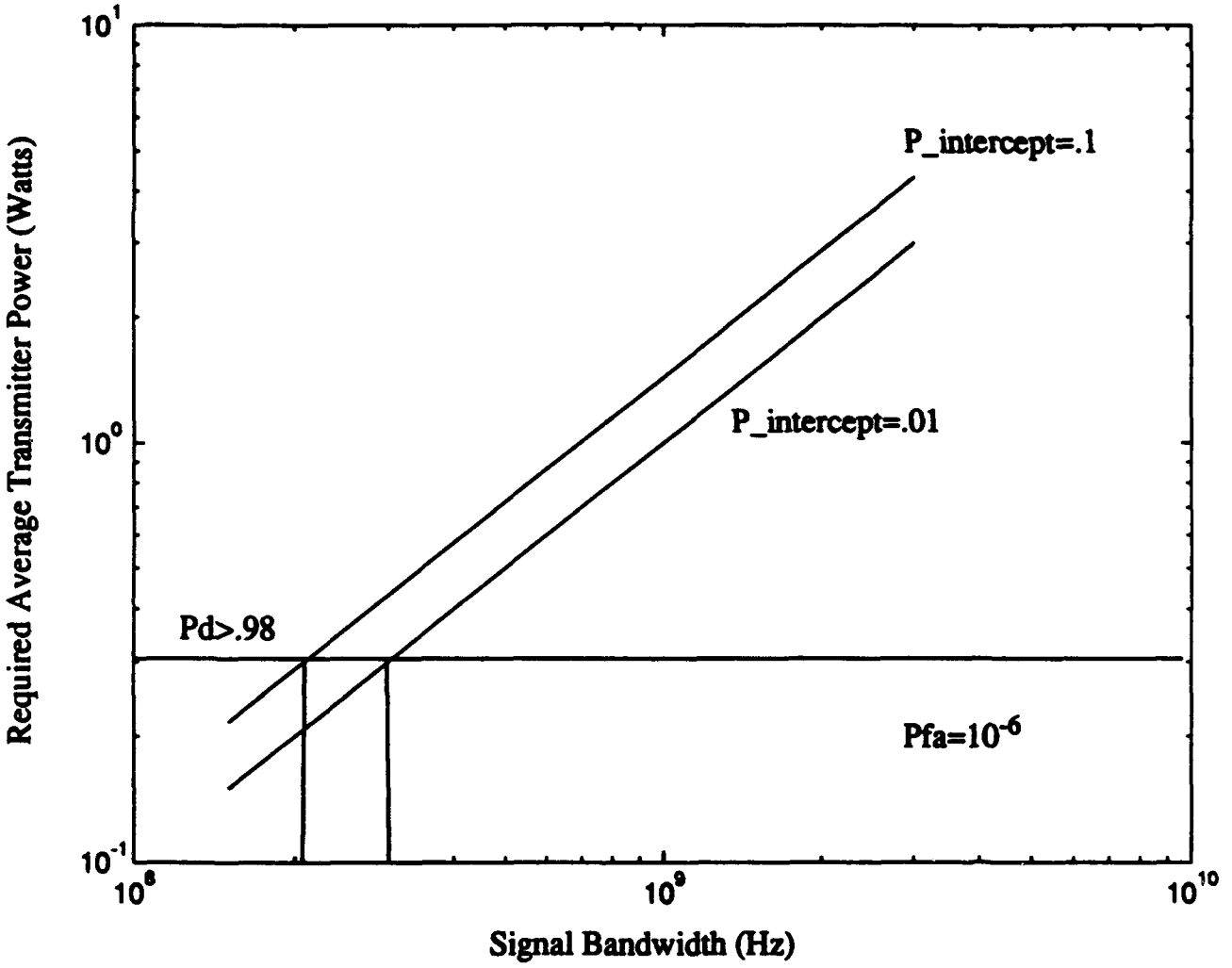

Figure 3-8. Average Power vs. Signal Bandwidth Trade-off for Radiometer Receiver Matched to Transmitter Pulse Width

spectrum, very high tracking performance can be obtained with low probability of intercept. The average transmitter power must be reduced to below 1 Watt to maintain a signal bandwidth below 1 GHz. Limiting the signal bandwidth to 500 MHz requires the average transmitter power to be below 600 mWatts. These results are tempered by the type of intercept receiver assumed in this analysis.

3.3 REFERENCES

[3.1] R.C. Dixon, Spread Spectrum Systems, Wiley, New York, 1984.

[3.2] R.G. Wiley, Electronic Intelligence: The Interception of Radar Signals, Artech House, Dedham, MA, 1985.

[3.3] D.J. Torrieri, Principles of Military Communication Systems, Artech House, Dedham, MA, 1981.

[3.4] R.E. Collin, Antennas and Radiowave Propagation, McGraw Hill, New York, 1985, p. 328.

[3.5] Textron Defense Systems specifications of the AN/SPN-46(V) Precision Approach and Landing System, TDS-08-92-255, 1992.

4.0 TASK 7: MILLIMETER-WAVE IMAGING SYSTEMS

4.1 INTRODUCTION AND SUMMARY

The Navy is interested in the utility of radar images as an aid to the landing signal officer on a carrier, and the use of an inverse synthetic aperture radar (ISAR) is the most practical approach to obtaining such images. The carrier aircraft will be on a radial heading during the landing approach, and this geometry is not favorable for making ISAR images at microwave frequencies because the change in aspect angle is not large enough. At millimeter wavelengths, the aspect angle change needed is much smaller because of the shorter wavelength, and past programs have demonstrated that the random yaw of an aircraft will provide a sufficient change in aspect angle to form images of aircraft on radial headings [4.1,4.2,4.3].

Section 4.2 discusses the operational requirements. From the images, one would like to identify the target and determine whether the landing gear and tail hook are down out to ranges of three to five kilometers. Range and azimuth resolutions of about 1.5 meters or better and sufficient sensitivity are required. The generation of ISAR images based on the natural yaw of a target is somewhat uncertain, and additional data is required to assess the utility of millimeter-wave ISAR as a landing aid for carrier aircraft. Section 4.3 reviews the literature search made to uncover past work and briefly discusses the radar requirements.

A literature search and phone inquiries were made to determine what operational millimeter-wave ISAR systems could be used in a proof-of-concept data collection. Because the scope of the task was limited, it was possible to make inquiries only with the organizations which were the most likely to have a millimeter-wave ISAR capability. Responses to the phone inquiries were obtained from a number of organizations, and the only millimeter-wave ISAR found that is currently operational in the CONUS is the 49 GHz system at the Naval Command, Control and Ocean Surveillance Center at San Diego. This organization has already collected ISAR images of naval aircraft. The 35 GHz radar at Kwajalein, which has made ISAR images of aircraft in the past, was not considered because it is outside CONUS. The System Planning Corporation is expected to have the capability of making millimeter-wave ISAR images with its Mark IV system (built as a corporate asset) after a 35 GHz frequency extender is completed early next year.

A number of other organizations could make millimeter-wave ISAR images with additions to existing equipment; these organizations include ERIM, Flamm & Russell, the Georgia Tech Research Institute, the Hughes Aircraft Corporation, Lintek, Inc., and Metratek, Inc. The modifications required are the addition of a millimeter-wave front end to an existing ISAR which operates at a lower frequency or the addition of a tracking capability to millimeter-wave instrumentation presently used at an RCS range.

In Section 4.4, radar parameters are listed for the millimeter-wave ISAR systems which some of the organizations listed above could provide. No radar parameters were listed for the other systems because these systems were capable of providing a wide variety of waveforms and PRFs, and it was not readily apparent what the parameters of a millimeter-wave ISAR would be.

4.2 OPERATIONAL REQUIREMENTS

The Navy is interested in investigating the use of millimeter-wave radar systems to aid the landing signal officer in carrier landings in adverse weather. The information desired includes the type of aircraft in the landing pattern and whether or not its landing gear and tail hook are down. The planned approach is to make radar images and determine these facts from the images.

The A-6E Intruder is a typical carrier aircraft which would be imaged. This aircraft has a wing span of 16.15 m, a length of 16.69 m, and a height of 4.93 m; its approach speed for landing is 110 knots or 57 m/s. The radar must image this target in adverse weather out to a range of 3 to 5 kilometers on an approach which is approximately radial, and the images must be available at intervals of 10 to 20 seconds. Assuming that a resolution of approximately one tenth of the target wing span is required, the radar imaging system must have a resolution of about 1.5 m or less.

The radar should have sufficient sensitivity so that the tail hook and landing gear are visible in the images. Although no data on the radar cross section (RCS) of the tail hooks on naval aircraft is readily available, it is estimated that a minimum detectable RCS of -15 to -20 dBsm (dB relative to 1 square meter) would be desirable. The radar could be less sensitive if an RCS enhancement device were attached to the tail hook and landing gear. In order to make

images, the radar must acquire and track targets as they enter the landing pattern. Skin tracking is an obvious possibility, another radar or other sensor could provide tracking data, or the targets could carry beacons.

4.3 DISCUSSION

4.3.1 Literature Search

As the first step in the task, the ERIM Information Research Center made a computerized search of the DTIC and NTIS data bases, but this search was not particularly helpful because papers given at relevant meetings and symposiums were not listed. A search was also made of the recent papers given at the Antenna Measurement Techniques Association (AMTA) Symposia and at the Tri-Service Radar Symposia because these symposia often include recent developments in imaging radars.

The two most relevant papers found were presented at recent Tri-Service Radar Symposia. The first paper discussed images made of aircraft at a center frequency of 35 GHz with a radar operated by MIT Lincoln Laboratory for the Army at Kwajalein [4.1]. ISAR images were made of a Learjet on inbound headings using the random yaw of the aircraft to provide the aspect angle change. The other paper discussed RCS measurements and ISAR images made at the Naval Command, Control, and Ocean Surveillance Center at San Diego at frequencies between 49.0 and 49.5 GHz [4.2]. ISAR images were made during circular orbits, portions of a race track, and inbound passes; the inbound pass images again used the target's random yaw motion to provide the required aspect angle change. Reference 4.3 is an unclassified reference to similar work with a Piper Navajo. The papers at the AMTA meetings describe ground-to-air and air-to-air measurement systems capable of making ISAR images of aircraft in flight [4.4-4.7]. These systems, however, did not operate in the millimeter-wave band, and they utilized the change in aspect angle caused by intentional target motion to form the synthetic aperture.

4.4 TECHNICAL CONSIDERATIONS

The most practical approach to imaging an incoming aircraft on a radial heading is to use an ISAR. The possible alternative of forming an image with a narrow beam antenna and a raster

scan would require a large, expensive electronically scanned array with a large number of elements.

An ISAR obtains fine range resolution by transmitting a wide bandwidth ΔB:

$$P_r = \frac{kc}{2\Delta\beta}$$

where k is a constant near unity, and c is the velocity of light. The value of k depends on the amount of weighting used for range sidelobe reduction. A range resolution of 1 m requires a bandwidth of somewhat over 150 MHz. The azimuth resolution r_a depends on the wavelength λ and the change in aspect angle $\Delta\Theta$ over which the data is integrated.

$$P_a = \frac{k\lambda}{2\Delta\theta}$$

Here again k is a constant near unity which depends on the aperture weighting needed for azimuth sidelobe reduction.

A transmitted bandwidth of hundreds of megahertz is possible at microwave frequencies, and it is practical to obtain 30 cm range resolution or better. When a carrier aircraft is in its landing pattern, it is on a nearly radially inbound course, and the planned target trajectory will not result in the change in the aspect angle change needed to provide good azimuth resolution. As a result, any ISAR images formed results from the change in aspect angle cause by target yaw; one of the key issues is the frequency at which target yaw provides usable images. The advantage of operating at millimeter wavelengths is that a much smaller aspect angle is required to get good azimuth resolution. At 10 GHz, $\Delta\Theta$ is 0.859 degrees for 1 m resolution; at 35 GHz, $\Delta\Theta$ is 0.245 degrees; and at 95 GHz, $\Delta\Theta$ is 0.090 degrees. Thus, it is possible to make ISAR images with a small aspect angle change at short wavelengths.

The utility of ISAR images for the present application was discussed in a phone conversation with R. J. Dinger of the Naval Command, Control, and Ocean Surface Surveillance Center in San Diego. Mr. Dinger is a coauthor of References 4.2 and 4.3, and he has had practical experience in gathering ISAR images of naval aircraft at millimeter wavelengths. It is not presently possible to assess the utility of ISAR images as an aid to the landing signal

officer because suitable data is not available. No images have been made of carrier aircraft on a low speed radial approach with the tail hook and landing gear down; slow targets are apt to yaw more than fast targets. Mr. Dinger believes that 49 GHz is a high enough center frequency for the intended application and that target recognition is practical.

4.4.1 Radar Requirements

The next logical step in assessing the practicality of millimeter-wave ISAR images as a landing control aid is a data collection program to acquire a suitable data base. A discussion of some of the key requirements for the ISAR used in the data collection program follows:

4.4.1.1 Operating Frequency

The ISAR should have an operating frequency between about 35 and 94 GHz to minimize the aspect angle change required to form an image. Component availability and atmospheric attenuation would make operation above 94 GHz difficult. Operation in the oxygen absorption band at 60 GHz would also be difficult.

4.4.1.2 Resolution

The ISAR images should have range and azimuth resolutions of about 1 meter or less.

4.4.1.3 Operating Ranges

An operational ISAR must form images between some minimum and maximum range limits. The operating ranges for the ISAR in the data acquisition program are less stringent than for an operational system, and it should be possible to collect data at ranges between about 1 and 3 to 5 km. With an operational system, waveform and antenna beamwidth changes may be necessary to accommodate the changing range of the target.

4.4.1.4 Transmitted Wave Form

The transmitted waveform must have a bandwidth of 150 MHz or more to provide 1 m range resolution, and the duty cycle must be high enough to provide adequate average power. ISAR radars normally use either linear FM (chirp) or stepped frequency waveforms. There

should be no problem in making the PRF high enough to provide adequate data samples for ISAR imaging. The ISAR must, of course, be coherent to form images.

4.4.1.5 Target Acquisition and Tracking

The data acquisition system must have a means of acquiring and tracking the target during the data collection passes. The radar could have its own tracking capability, another radar or other sensor could supply tracking data, or the target could carry a beacon. The slew rate of the antenna pedestal must be rapid enough to track the target during normal landing maneuvers.

4.4.1.6 Sensitivity

The ISAR must have adequate sensitivity so that scatterers with some minimum RCS level are visible in images made at ranges of 3 to 5 km or more. The sensitivity is a function of the antenna gain, the average transmitted power, the system losses, the receiver noise temperature, the atmospheric loss, and the integration time. The minimum scatterer RCS required is estimated to be about -15 to -20 dBsm for an operational system; this number can be estimated with better accuracy after a data base is acquired.

4.4.1.7 Antenna Polarization and Beamwidth

The capability of transmitting and receiving either linear or circular polarization during the acquisition of the image data base would be desirable. Circular polarization is often used to reduce rain clutter in bad weather at lower frequencies, and some circularly polarized images could be made if circular polarization might be used in an operational system.

The spot size of the antenna beam must be reasonably well matched to the target span. If the beam is too narrow, parts of the target will be missing in the image, and if the beam is too broad, a high average transmitter power will be necessary for long range operation. If a single antenna is used at all ranges, it should have a wide enough beamwidth so that the spot size at the minimum range includes the entire target. A 1 degree beamwidth would have a spot 20 m wide at a range of 1146 m; hence, a 1 degree beam would be reasonable for the data base acquisition. With an operational system, it may be necessary to use a narrower beam and spoil the beam at short range.

4.4.1.8 Processing Capability

Although real time image formation is a necessity for an operational system, data could be recorded and processed off-line during the database acquisition. The ISAR imaging system must have the capability of forming images from the recorded data. Since the target translation and rotation are unknown, the processing will require that there be isolated or dominant scatterers in the return. There must be at least one prominent point; the ERIM prominent point processing algorithm normally uses two prominent points [4.8]. With the ERIM algorithm, the data is first compressed in range, and a prominent point is tracked in azimuth to eliminate translational effect; this prominent point becomes the new focused scene center. The algorithm then unwraps the phase of a second prominent point in azimuth, and uses the unwrapped phase to eliminate spatially variant errors resulting from non-uniform motion.

4.4.2 Equipment Available

4.4.2.1 Discussion

After the literature search and suggestions from ERIM personnel knowledgeable in ISAR systems, a list was made of organizations that are the most likely to have millimeter-wave ISAR systems or ISAR systems operating at lower frequencies which could be easily modified to provide a millimeter-wave ISAR capability. Phone calls were then made to the organizations on the list to determine the suitability of their ISAR systems, and additional information was requested. Because of the limited scope of the task, it was not possible to contact all possible organizations which might have ISAR systems suitable for imaging naval aircraft. The following organizations, listed alphabetically, have existing instrumentation or instrumentation which could be modified to make millimeter-wave ISAR images:

1. ERIM
2. Flamm and Russell, Inc.
3. Georgia Tech Research Institute
4. Hughes Aircraft Corporation
5. Lintek, Inc.
6. Metratek, Inc.
7. Naval Command, Control and Ocean Surveillance Center
8. System Planning Corporation

Phone calls were also made to the MIT Lincoln Laboratory and the Navy's Pacific Missile Test Center at Point Mugu, but these organizations did not have instrumentation suitable for imaging aircraft in flight. Discussions of the ISAR instrumentation from the organizations listed above follows.

4.4.2.2 ERIM

An ERIM point of contact is:

James Steinbacher
Environmental Research Institute of Michigan
P.O. Box 134001
Ann Arbor, Michigan 48113-4001
Area 313 994-1200

ERIM is now in the final stages of the Ground-to-Air Imaging Radar (GAIR) program and will soon deliver this system to the Nellis Air Force Base; Reference 4.8 has a more detailed system description. The GAIR system was developed for the Air Force to image airborne targets, especially low observable aircraft. A unique feature of this system is the capability of collecting total radar cross section data simultaneously with ISAR image data. Although the GAIR system currently collects data only at X-band, the system architecture was designed to allow the addition of other RF front ends. An RF front end could be added for operation at 35 GHz, 94 GHz, or anywhere else in the millimeter-wave band. Since the millimeter-wave antenna would be small, it could be mounted above the existing X-band antenna on the same pedestal.

A video camera provides angular tracking data, and the radar return is processed for range tracking. Prominent point processing software has been tested and images have been made of the F-117 and other aircraft, consequently, proven software is available for forming ISAR images of naval aircraft. The GAIR system is fully calibrated, fully transportable, and capable of remote operation using mobile generator power. Although the GAIR will normally be located at the Nellis AFB, the GAIR will be available for other government programs. The expected GAIR parameters with a Ka-band front end are as follows:

Parameters for GAIR Operation at Ka-band

Center frequency	35 GHz
Processed bandwidth	600 MHz
Range resolution	30 cm
Azimuth resolution	dependent on integration angle
Peak transmitted power	1000 W
Waveform	linear FM (chirp)
Pulse widths	12.7 msec at long range 6.34 msec at intermediate ranges 1.054 msec at short range
PRF	10,000 Hz
Noise figure and losses	14 dB
Range window	100 m

4.4.2.3 Flamm and Russell, Inc.

A point of contact for Flamm and Russell is:

Mr. Bradley W. Deats
Flam & Russell, Inc., Western Operations
P.O. Box 5263
Englewood, CO 80112-5263
Area 303 649-9300

Flamm and Russell's capabilities were discussed during a phone conversation with Mr. Bradley Deats. Flamm and Russell has built low power millimeter-wave instrumentation operating in the 26.5 - 40 GHz band for a controlled environment; this instrumentation, which uses a stepped frequency, gated CW waveform, might be suitable for proof-of-concept experiments. Flamm and Russell also has constructed an X-band system with wide-band chirp which is housed in a trailer. This system, which was built for NADC, can track incoming targets, but it will require an upconverter to make millimeter-wave ISAR images of aircraft.

4.4.2.4 Georgia Tech Research Institute

A point of contact for Georgia Tech is:

Ted Lane
Georgia Tech Research Institute
Georgia Institute of Technology
Atlanta, Georgia 30332-0800
Area 404 528-7682

The Georgia Tech Research Institute (GTRI) millimeter-wave imaging capabilities were discussed with Mr. Nick Currie. GTRI has a coherent millimeter-wave instrumentation radar which operates at two frequencies, 35 and 95 GHz; this radar can provide ISAR images or high resolution range profiles of targets on a rotary platform on an instrumentation range. The radar uses a stepped frequency waveform. Although the radar can not track airborne targets at present, the addition of a monopulse antenna and additional receiver components would provide a tracking capability. Some of the key system parameters are listed in the table below.

GTRI MMW Instrumentation Radar Transmitter and Antenna Parameters

Parameter	35 GHz Characteristics	95 GHz Characteristics
Transmitter		
Frequency	34.75-35.75 GHz	93.0-95.0 GHz
RF Agile BW	1 GHz Coherent	2 GHz Coherent
Frequency Step	8 MHz	8 MHz
Peak Power	3 W	80 W
Pulse Width	70 ns	70 ns
PRF	35 kHz	50 kHz
Resolution	8 inches	4 inches
Antenna		
Type	4.5 inch lens	1.5 inch lens
Beam	6 degree Pencil Beam	6 degree Pencil Beam
Gain	29 dB	29 dB

Sidelobes	25 dB below main lobe	25 dB below main lobe
Polarization	Dual Polarized	Dual Polarized
Transmit	Linear or Circular	Linear or circular
Receive	Simultaneous 2 Channel	Simultaneous 2 Channel

4.4.2.5 Hughes Aircraft Company

A point of contact for Hughes is:

Calvin R. Boerman
Hughes Aircraft Company
P.O. Box 92426
Los Angles, CA 90009
Area 310 334-8304

The Hughes capabilities were discussed with Cal Boerman of Hughes. Hughes has an X-band data collection system, which, housed in a trailer, has collected ISAR images of a Mooney 231 aircraft; this radar uses a stepped frequency waveform [4.6]. Although this system does not currently have a millimeter-wave capability, Hughes has built and delivered 35 GHz front ends in the past, and Hughes could construct a similar front end to provide a millimeter-wave capability for the system.

4.4.2.6 Lintek, Inc.

A point of contact for Lintek, Inc. is:

Dr. Daniel Fleisch
Lintek, Inc.
60 Grace Drive South
Powell, Ohio 43065
Area 614 888-2700

Lintek instrumentation was discussed on the phone with Dr. Fleisch. Lintek has a product line of radar measurement instrumentation which is phase coherent and compatible with real-time and off-line ISAR processing with software supplied by other organizations such as CompuQuest

and ISAR, Inc. Lintek measurement systems have been delivered to a number of government laboratories and corporations in the defense business.

This radar instrumentation now operates at frequencies between 100 MHz and 35 GHz, but Lintek is currently working on extending the operating range to 100 GHz. The standard Lintek systems are normally used on static RCS measurement ranges, but the systems were designed to make it easy to add additional capabilities. The ability to support target tracking was designed into the hardware of the Lintek elan measurement system, and Dr. Fleisch felt that the software modifications to support target tracking would be low risk. He also stated that the processing speed of the computing system would allow the tracking of vehicles in highly dynamic trajectories. Tracking could be done on the radar data or with an external tracking system; a tracking pedestal and a suitable millimeter-wave antenna would, of course, be required. Position data and radar data could be interleaved.

The specifications of the Lintek elan radar cross section measurement system indicate that system is wide band and that it supports multiple complex waveforms and a variety of PRFs. TWT output stages can be added to supply up to a kilowatt of output power. Further discussions with Lintek are needed to determine what the recommended transmitter waveform and other operating parameters would be for a Lintek supplied system.

4.4.2.7 Metratek, Inc.

The Metratek point of contact is:

Mr. Ray Harris
Metratek, Inc.
12330 Pinecrest Road
Reston, VA 22091
Area 703 620-9500

Metratek has built a number of radar systems over the past few years, and all of these systems are coherent SAR, ISAR, or AIRSAR (Autofocus Imaging Systems). The Metratek Model 100 AIRSPAR, which covers the 8 - 18 GHz and lower frequency bands is currently installed in an A-3. Ray Harris stated that Metratek, Inc. could build one of their standard Models 100, 200 or 300 for the present ISAR imaging application but that Metratek would have to build a millimeter-wave front end for whatever model is selected. There would, of course,

be a cost and delivery time associated with the construction of a millimeter-wave front end. Further discussions with Metratek are needed to finalize the data collection parameters.

4.4.2.8 Naval Command, Control and Ocean Surveillance Center

A point of contact for this organization is:

R. J. Dinger
Naval Command, Control, and Ocean Surveillance Center
RDT & E Division (NRaD)
San Diego, California 92152
Area 619 553-2500

The Naval Command, Control, and Ocean Surveillance Center has equipment and experience which is directly applicable to the collection of proof of concept data to determine the utility of ISAR images as a carrier aircraft landing aid. This organization has already collected ISAR images of naval aircraft on inbound and other headings at a frequency of 49 GHz [4.2,4.3]. They currently have an operational millimeter-wave radar which can form ISAR images, and Mr. Dinger said that they are well positioned to take more ISAR data since naval aircraft are close by. The parameters for this radar are given in the table.

Parameters of Navy 49 GHJz ISAR Radar
(from Reference 4.2)

Frequency Range	49.0 - 49.5 GHz
Bandwidth	0.5 GHz
Waveform	Stepped Frequency 32 to 512 Steps
Peak Pulse Power	40 W from TWT
Pulse Width	5 msec Typical
PrF	10,000
Duty Factor	.05 Typical
Polarization	Vertical or Horizontal
Receiver	2 Channel, Co- and Cross-Polarized

Antenna	
Type	2 with Cassegrain Feed Parabolic
Diameter	45 cm
Beamwidth	1 Degree
Minimum Meas. RCS	-22 dBsm at 1 nmi -4 dBsm at 2 nmi

4.4.2.9 System Planning Corporation

A point of contact for System Planning Corporation (SPC) is:

Mr. Jeffrey B. Floyd
System Planning Corporation
1429 N. Quincy Street
Arlington, Virginia 22207-3645
Area 703 351-8653

SPC has delivered a number of their Mark IV coherent pulsed RCS and antenna measurement systems to a variety of customers. These systems, which use pulse-to-pulse frequency stepping, and the associated software can provide ISAR images with real-time or off-line processing. The System Planning Corporation has built three of the Mark IV systems as corporate assets, and a Mark IV could be deployed for field ISAR measurements of naval aircraft. RF frequency converters covering 0.1 to 18 GHz and 35 GHz are in service. SPC has built a 35 GHz system for the NWC with two different transmit power levels: 1 kW at 0.5 GHz bandwidth and 70 W at 2 GHz bandwidth. SPC is currently building a 35 GHz frequency extender for use with one of the corporate radars, and this frequency extender is expected to be ready by the end of the year. SPC has also designed and built a 60-GHz extender with a 0.1 W power level and a 5 GHz bandwidth for a corporate radar. SPC has designed and partially built a 95 GHz extender for the Army which provides 5 W with a 1 GHz bandwidth, but the completion data for this extender is further out in time.

With the completion of the 35 GHz frequency extender, SPC will have a corporate radar capable of making ISAR images of aircraft at 35 GHz. Further discussions with SPC are needed to determine what the operating parameters of their system would be.

4.5 REFERENCES

[4.1] D.W. Kerr, B.Y. Koo, and C.H. Chen, "Inverse Synthetic Aperture Radar (ISAR) Imaging of a Non-Maneuvering Aircraft (U), "Record of the 35th Annual Tri-Service Radar Symposium, Report Number WRDC-TR-89-1142, ERIM, Box 134001, Ann Arbor, MI 48113-4001, January 1990 (SECRET).

[4.2] R.J. Dinger, G. Kinzel, and S. Jones, "Measurements of the Radar Cross Section and Inverse Synthetic Aperture Radar Images of Piper Navajo at 9.5 and 49 GHz," Naval Command, Control, and Ocean Surveillance Center/RDT&E Div (NRaD), TD 1569, January 1993 (UNCLASSIFIED).

[4.3] R.J. Dinger, et al., "Radar Cross Section and ISAR Images of Flying Aircraft at 49 GHz (U)," presented at the 39th Annual Tri-Service Radar Symposium, Monterey, CA, June 1993 (SECRET). (Symposium record in press, available from ERIM in the future).

[4.4] C.T. Nadovich, J.F. Aubin, and D.R. Frey, "An Instrumentation Radar System for Use in Dynamic Signature Measurements," presented at the 14th Antenna Measurement Techniques Association Meeting and Symposium, Columbus, Ohio, October 1992.

[4.5] R. Harris, et al., "Dynamic Air-to-Air Imaging Measurement System," presented at the 14th Antenna Measurement Techniques Association Meeting Symposium, Columbus, Ohio, October 1992.

[4.6] A. Jain and I. Patel, "ISAR Imaging of Aircraft-in-Flight Using Ground-Based and Airborne Radars", presented at the 14th Antenna Measurement Techniques Associatiion Meeting and Symposium, Columbus, Ohio, October 1992.

[4.7] A.D. Siegel, "Dynamic Helicopter Radar Signatures", presented at the 13th Antenna Measurement Techniques Association Meeting and Symposium, Boulder, Colorado, October 1991.

[4.8] S. Crippen, et al., "A High Performance Inverse Synthetic Aperture Radar System for Imaging Low Observable Airborne Targets (U)," presented at the 39th Annual Tri-Service Radar Symposium, Monterey, CA, June 1993 (SECRET). (Symposium record in press, available from ERIM in the future).

5.0 TASK 8: WIND DETECTION

5.1 SUMMARY AND CONCLUSIONS

5.1.1 Summary

The Navy is interested in the feasibility of using a radar sensor for measuring wind speed near the flight deck of an aircraft carrier or amphibious assault ship, or near the helicopter landing platforms of smaller ships. This is a difficult problem because the volume backscatter of clear air is very low. A preliminary design was made for a radar wind sensor operating at C-band. Even though the strawman radar wind sensor transmitted a long pulse and used a high duty cycle, the peak and average power needed to detect volume backscatter from clear air were very high. Another problem was that a large amount of clutter suppression was required; it may not be possible to get an adequate amount of sea clutter suppression from a moving ship.

5.1.2 Conclusions

Building a radar wind sensor for shipboard use appears to be possible, but the use of a radar wind sensor is an unattractive solution to the wind measurement problem for the following reasons:

- The radar will require a transmitter with a very high output power to detect the faint echoes from clear air, and such a transmitter will be large, bulky, expensive, and difficult to maintain.

- The high transmitter power will also present a significant radiation hazard, and the radar beam should not be scanned near any personnel.

- For the radar wind sensor to work properly, a large amount of sea clutter suppression will be required. Obtaining sufficient clutter suppression from a moving ship at sea presents a significant technical risk; algorithms developed for land-based weather radars will not be suitable. Sophisticated subsystems and processing algorithms will be needed to provide the required clutter suppression. The antennas must be designed to have low sidelobes below boresight to minimize the clutter received through the sidelobe, and the antenna elevation angle must be high enough to minimize clutter reception through the sidelobes.

- The radar will be complex and sophisticated, and its design, construction, and testing will require significant financial resources. The radar will require well trained personnel for shipboard operation, and it will take up a considerable volume.

- Few climatological studies of the refractive index structure constant are available, and the percentage of time the reflectivity is high enough for wind measurements is unknown. The reflectivity varies with the area in the world.

5.2 STATEMENT OF PROBLEM

The Navy is currently using anemometers mounted on ship superstructures to measure wind velocities; however, the wind near the superstructure is not the same as the wind over the flight deck or a landing platform. Thus, the Navy has an interest in developing instrumentation to measure the wind speed and direction remotely to provide more accurate wind data for the flight deck of an aircraft carrier, amphibious assault ship, or a helicopter landing platform on a guided missile cruiser or destroyer. Since weather radars have been in use since the 1950s [5.1], it is natural to investigate the possibility of making wind measurements using some portion of the RF spectrum.

There are a number of meteorological radars currently in use [5.2,5.3]. The National Weather Service and the Air Weather Service operate the WSR-88D, the next generation of weather radar, which furnishes reflectivity and radial velocity data to provide storm warnings and hydrology measurements [5.4]. The Federal Aviation Administration has deployed the terminal Doppler weather radar (TDWR) system to provide automatic detection of microburst-induced windshear near airports [5.5]. Radar sensors operating at UHF and VHF frequencies have been in use for some time to study the structure and dynamics of the troposphere and stratosphere [5.6]. Airborne weather radars operating at C- or X-band provide long range weather detection. The minimum operating ranges for conventional meteorological radars are typically one hundred kilometers or more, while wind profiling radars, which measure winds in the vertical direction, receive returns from altitudes of tens of kilometers. During the limited literature search conducted for this task, no mention was found of a wind velocity measurement system operating at the very short ranges required for this task.

The use of shipboard radar wind measurement sensors was discussed with NAWC personnel [5.7]. The Navy is also looking at laser Doppler radar sensors for making the wind measurements. The Navy requirements are quite different than those of conventional meteorological radars. Figure 5-1 is a sketch of the approximate search volume desired for the sensor. Wind speed measurements are needed from a minimum range of 20 to 50 meters to

a maximum range of about two kilometers with 360 degree angular coverage; however, the top priority search volume is an arc of about 90 degrees to the rear of a ship where fixed wing aircraft or helicopters are coming in for a landing. Measurements are needed at heights above sea level of 10 to 100 meters. The Navy has not specified the velocity measurement accuracy required, but a reasonable goal is one meter/second. The ship speeds expected are approximately 10 to 30 knots.

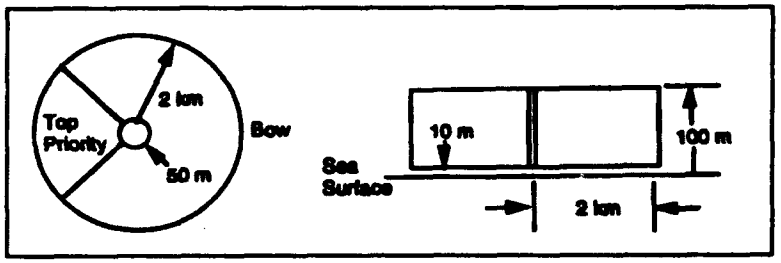

Figure 5-1. Approximate Search Volume

Figure 5-2 is a sketch of the geometry for a wind sensor mounted on a Nimitz class aircraft carrier. The radar wind sensor will be mounted on the rear of the island approximately 90 meters from the stern. The flight deck of the carrier is about 23 m above the ocean surface, and the sensor will be 18 to 32 m above the flight deck. Although the primary purpose of the sensor is the measurement of radial wind speeds to the rear of the carrier along the flight path of aircraft coming in for a landing, the sensor can also measure radial wind speeds at other angles where there are no obstructions to a clear line-of-sight. The geometry for amphibious assault ships is similar to that of a carrier.

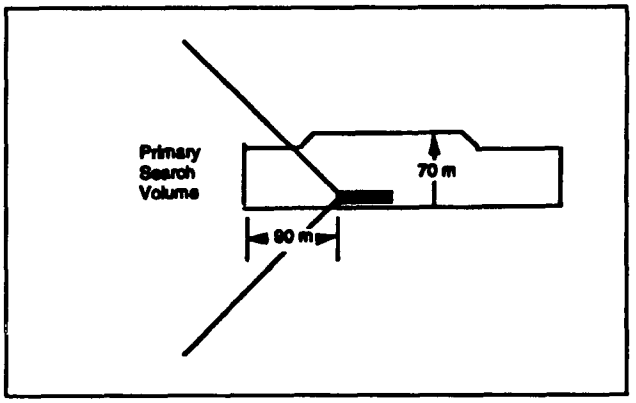

Figure 5-2. Wind Sensor on Carrier Deck 23 Meters Above Sea Surface. Sensor 18-32 m above deck.

Wind velocity measurements are also of interest for cruisers, destroyers, and frigates as an aid for helicopter landings. Figure 5-3 has a sketch of a typical geometry for a frigate. The wind sensor will be located above the landing platform at the stem about ten meters above sea level 28 meters from the stern; it will measure radial wind velocities in the rear or to the side of the ship, but not toward the bow because of the presence of the superstructure. A guided missile cruiser is a larger ship, and the wind sensor on a cruiser would be located about 56 meters from the stern about 20 meters above sea level.

5.3 WEATHER ECHO

5.3.1 The Weather Radar Equation

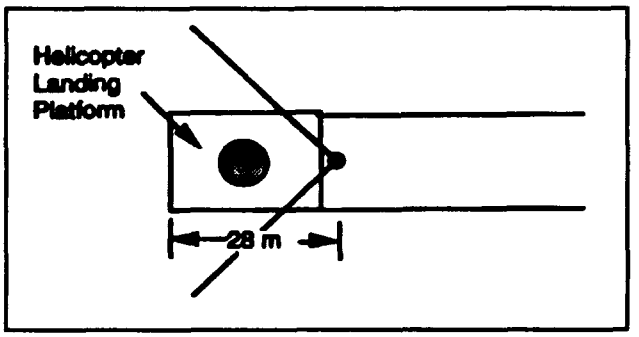

Figure 5-3. Typical Geometry for a Frigate

The major distinction between meteorological radars and other radars is the nature of the target; meteorological targets are distributed in space, and the radar returns come from a volume. Although precipitation is a major source of volumetric backscatter, backscatter from chaff, birds, or insects can also occur. There is, of course, no precipitation in clear air, but there are backscatter and reflections from inhomogeneities in the refractive index.

When scatterers fill the radar beam, the sample volume V is approximately

$$V \approx \frac{\pi \cdot \theta \cdot \phi \cdot R^2 \cdot \rho_r}{4}$$

where θ and ϕ are the azimuth and elevation beamwidths, R is the range to the volume, ρ_r is the range resolution. With a pulsed radar, the range resolution is

$$\rho_r = \frac{c \cdot \tau}{2}$$

where c is the velocity of light and τ is the pulse width. When pulse compression is used

$$\rho_r = \frac{c}{2 \cdot \Delta B}$$

where ΔB is the transmitted bandwidth. The radar cross section (RCS) σ of the volume is

$$\sigma = \eta \cdot V$$

Here σ is the RCS in square meters per cubic meter. If the radar RCS is substituted in the standard radar equation, the return power can be calculated. The return power can also be computed from the general form of the weather radar equation.

$$P_r = \frac{P_t G^2 \lambda^2 \eta}{(4\pi)^3 R^2 L} \cdot \frac{(\pi\theta^2)}{(8\ln 2)} \frac{c\tau}{2}$$

where P_r = the received power in W

P_t = the peak transmitted power in W

G = the antenna gain

λ = the wavelength in m

η = the reflectivity per unit volume in m^2/m^3

R = the range to the volume in m

L = losses (L > 1) from the atmosphere, RF attenuation, and receiver mismatch

θ = 3dB antenna beamwidth in radians

c = velocity of light

τ = pulse width in s

This equation was derived by assuming a circularly symmetrical Gaussian antenna beam, and the $\pi/8\ln 2$ factor in the second bracketed quantity results from this assumption.

Radar meteorologists usually relate η to factors having meteorological significance. In 1908 Mie developed a theory for the energy backscattered from spherical droplets by a plane wave; the energy is a function of the wavelength, the complex index of refraction of the droplets, and the ratio of droplet circumference to the wavelength. When the scattering from the droplets is in the Rayleigh region; i. e., the wavelength is large compared to the droplet radius:

$$\eta = \frac{\pi^5}{\lambda^4} |K_w|^2 Z$$

The reflectivity factor Z is the sum of the droplet diameters D_i raised to the sixth power in the volume ΔV

$$Z = \frac{1}{\Delta V} \sum_i D_i^6$$

Normally Z is given in units of mm^6/m^3 by radar meteorologists. In the previous equation, $|K_w|^2$, which is related to the complex index of refraction of water, is approximately 0.93 at temperatures between 0 and 20 degrees C. At wavelengths short enough so that the Rayleigh

approximation does not apply, it is customary to replace Z by Z_e where Z_e is the effective reflectivity factor. Meteorologists normally use a logarithmic scale for Z, and in logarithmic units dBZ = 10 $\log_{10}$ Z.

The weather radar equation can also be rewritten in terms of the effective reflectivity

$$P_r = \frac{10^{-18}\pi^3 P_t G^2 \theta^2 c\tau |K_w|^2 Z_e}{2^{10}(\ln 2)\lambda^2 R^2 L}$$

Here all the terms are in MKS units except that Z_e is expressed in units of (millimeters)^6 per cubic meter; the factor of 10^{-18} on the right side accounts for these Z_e units.

5.3.2 The Reflectivity of Volume Backscatter

An expression frequently used for Z in the presence of rain in temperate latitudes is:

$$Z = 200 \cdot r^{1.6}$$

Here r is the rain rate in millimeters per hour. For moderate rain, r = 4 mm/hr, the reflectivity is 33 dBZ, and $\eta = 4.04 \times 10^{-8}$ m^2/m^3 at a 5.5 cm wavelength (after multiplying Z by 10^{-13} to convert to MKS units). For light rain at 1 mm/hr, the reflectivity is 23 dBZ, and $\eta = 4.4 \times 10^{-9}$ m^2/m^3. Radars used for the detection of wind shear must detect reflectivities less than 0 dBZ[5.8]; $\eta = 2.2 \times 10^{-11}$ m^2/m^3 for 0 dBZ.

Radars can detect echoes from inhomogeneities in the atmosphere caused by turbulence. Variations in the refractive index η are directly related to variations in atmospheric moisture, temperature and pressure, and atmospheric turbulence changes the refractive index which causes backscattering. The radar reflectivity η resulting from Bragg backscatter caused by isotropic turbulence in the inertial subrange is

$$\eta = 0.38\, C_n^2\, \lambda^{-\frac{1}{3}}$$

where C_n^2 is the refractive index structure constant which is related to the mean square fluctuations of the refractive index, and λ is the wavelength. According to turbulence theory, there is a range of eddy sizes where the kinetic energy of the eddies dominates over the dissipation due to viscosity, and the turbulence is essentially isotropic; this is the inertial subrange. In the dissipative range, eddies are smaller in size, and energy is dissipated into heat because of viscosity.

Although this equation is often used to predict backscatter from clear air, the assumption that the turbulence is isotropic is questionable at short wavelengths. There is a critical wavelength below which the theory does not apply, and the reflectivity is less than what is predicted. The critical wavelength is about four times the inner scale of the inertial subrange; the critical wavelength could increase from two or three cm. with a high eddy dissipation rate to twelve centimeters with a low eddy dissipation rate.

The table below lists some typical volume reflectivities for C-band operation; note the wide variation between the reflectivities of rain and those of clear air. The clear air reflectivity values were computed using the above equation and a wavelength of 6 centimeters.

The C_n^2 values depend on temperature and humidity gradients as well as on the turbulence. Unfortunately, few climatological studies of C_n^2 exist [5.9]. Doviak has a plot of the median value of C_n^2 for maritime air from a 1977 reference [5.10]; the median value was $3.9 \times 10^{-15} \exp(-h/2)\ m^{-2/3}$, where h is the height in kilometers. At sea level, $\eta = 3.9 \times 10^{-15}\ m^2/m^3$ at a wavelength of 5.5 cm. Airborne measurements made in Florida in October at 9.4 GHz showed that C_n^2 was about $10^{-13}\ m^{-2/3}$ at sea level [5.11]. Andreas [5.12] calculated C_n^2 statistics for drifting ice over the Beaufort Sea at a height of two meters above the ice surface; the calculations were made from meteorological data collected every six hours for a year. At radio frequencies, the average C_n^2 values were 3.5×10^{-14}, 1.1×10^{-14}, 3.0×10^{-14}, and $1.5 \times 10^{-14}\ m^{-2/3}$ for spring, summer, autumn, and winter, respectively. An analysis of the histograms in indicate that approximately 22%, 40%, 33% and 19% of the time, C_n^2 was below $2 \times 10^{-15}\ m^{-2/3}$ for the spring, summer, autumn, and winter seasons, respectively.

Selecting a reflectivity value for use in designing a wind sensor is difficult because C_n^2 varies widely with conditions, and measured values can vary by an order of magnitude above or below the median value with changes in the weather. An η value of $4 \times 10^{-15}\ m^2/m^3$ will be

assumed for C-band operation for design purposes, although the backscatter could be much more or less.

η (m^2/m^3)	Conditions
4×10^{-8}	Moderate rain, 4 mm/hr
4.4×10^{-9}	Light rain, 1 mm/hr
2.2×10^{-11}	Approx. minimum for "dry" microburst
2.9×10^{-13}	Strong turbulence
1.9×10^{-15}	Intermediate turbulence
$5.8\ 10^{-17}$	Light turbulence

In any event, the volume backscatter from clear air is very low which makes detection difficult. For example, if the volume V is 100 cubic meters, and η is 4×10^{-15}, the RCS of the volume is 4×10^{-13} m^2 or -124 dBsm. For perspective, the approximate RCS of a standing man is about 0 dBsm, and the approximate RCS of a sparrow is -30 dBsm.

5.4 DESIGN CONSIDERATIONS

5.4.1 PRF and the Operating Frequency

When data is sampled at a fixed rate, the highest frequency which can be sampled unambiguously is the Nyquist frequency which equals half the sampling rate. Thus, if the radar pulse repetition frequency (PRF) is fixed, the highest Doppler frequency Δf_d which can be measured unambiguously equals half the PRF:

$$\Delta f_d = \pm \frac{PRF}{2}$$

The Doppler shift f_d equals twice the radial velocity V_r divided by the wavelength λ

$$f_d = \frac{2V_r}{\lambda}$$

Combining these equations, the maximum radial velocity V_a which can be measured unambiguously is proportional to the product of the wavelength and the PRF:

$$V_a = \pm \frac{\lambda PRF}{4}$$

Range ambiguities occur when the radar receives returns from near range from the pulse transmitted most recently along with returns from longer ranges from previous pulses. The unambiguous range ΔR depends on the time T_s between pulses, 1/PRF, and the velocity of light c:

$$\Delta R = \frac{c}{2 \cdot PRF}$$

Thus, raising the PRF to increase the maximum unambiguous radial velocity reduces the unambiguous range interval. Some weather radars use dual pulse repetition frequencies to resolve range and Doppler ambiguities.

The choice of the operating frequency for a weather radar is a compromise between a number of factors. Radars which measure vertical wind profiles have center frequencies at 40 to 50 MHz, 400 MHz, or 915 MHz, while long range storm warning radars operate at S-band near 3 GHz or C-band near 5.5 GHz. Airborne storm warning radars operate at either C-band or X-band near 10 GHz. Radars used for work with clouds may operate at millimeter wavelengths [5.13]. A C-band operating frequency appears to be a good choice for the ship wind sensor. The wavelength is long enough so that 1) the reflectivity is probably reasonably close to that predicted above, and 2) the sampling requirements for unambiguous radial velocities can be met. Operation at a lower frequency, such as S-band, would require antennas with too large an aperture.

As discussed above, the choice of the PRF is a compromise between measuring Doppler shifts unambiguously and the unambiguous range interval. Assuming a 5.5 GHz center frequency, the wavelength will be 0.0545 m. With a PRF of 4000, the unambiguous radial velocity which can be measured will be 54.5 m/s (106 knots). The unambiguous range interval will be 37.5 km.

5.4.2 Search Volume and Resolution

One typical operational scenario is likely to be similar to that sketched in Figure 5-4. The radar scans a 90 degree sector at the rear of the ship with a pencil beam antenna; the scans could be at a single elevation angle or the elevation angle could change from scan to scan. A typical 3 dB antenna beamwidth is two degrees (35 mrad), which results in 45 angular resolution cells across the 90 degree sector. At the maximum desired range of two kilometers, the antenna spot size will be 70 meters which is approximately equal to the vertical coverage desired. As will be discussed later, sea clutter will limit the minimum volume scatter which can be detected. Since the radar will receive sea clutter through the antenna sidelobes, the radar antenna must point far enough above the horizontal so that the antenna gain is low for the sea surface. The minimum elevation angle will have to be at least 2 or 3 degrees to keep the sea surface in the sidelobe region of the antenna. Measurements within 10 meters of the sea surface are not feasible at any significant range because of antenna sidelobes.

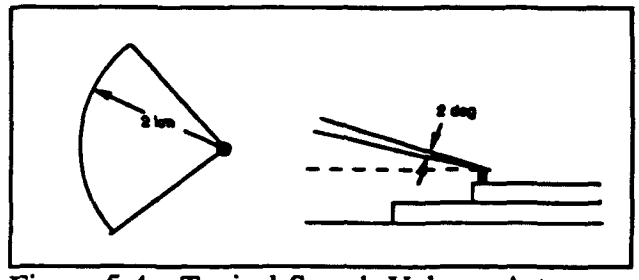

Figure 5-4. Typical Search Volume Astern

The choice of the resolution cell volume is a compromise. If the cell volume is too small, the RCS will be low and hard to measure, while if the cell volume is too large, it will be difficult to tell how the wind speed varies with the location. A range resolution of 10 meters is proposed to provide a reasonable compromise between these two factors. There will be approximately 200 range cells between the minimum range of about 50 meters to the maximum range of 2000 meters.

A scan rate of nine degrees/second will be assumed so that 10 seconds will be required to scan the 90 degree sector. Assuming a PRF of 4000 Hz and that 100 samples are used to make a velocity estimate, the antenna beam position will change by 0.22 degrees during the collection of 100 data samples.

5.4.3 Pulse Pair Processing and Signal-to-Noise Ratio Requirement

Weather radars measure the following quantities:

- the echo power, which provides an indication of the liquid water content of hydrometers or the reflectivity of clear air,
- the mean Doppler velocity, which indicates air motion toward or away from the radar, and
- the spectrum width, which is a measure of the velocity dispersion within the resolution cell

The mean Doppler velocity is the quantity which is of primary interest for a wind sensor on a ship. The methods of mean frequency extraction which have been implemented on meteorological radars are based either on the autocovariance or the discrete Fourier transform of the complex data samples at the receiver output. Since a pulse-pair processor is less complex and costly than a fast Fourier transform (FFT) processor, we shall assume that the ship wind sensor will use pulse-pair processing. Pulse-pair processing estimates the mean Doppler velocity and Doppler spectral width from the autocovariance function at a lag of T_s [5.14].

Reference 5.1 has plots of the standard deviation of the mean Doppler frequency estimate as a function of the normalized spectrum width for single pulse signal-to-noise ratios of -5 dB, 0 dB, and 20 dB or more. The normalized spectrum width σ_{vn} is

$$\sigma_{vn} = \frac{\sigma_v}{2v_a}$$

where σ_v is the width of the Doppler spectrum, and v_a is the unambiguous velocity. The spectrum width σ_v is variable, but based on chaff measurements, a reasonable value to assume is 1 m/s. With an unambiguous velocity of 54.5 m/s, σ_{vn} is on the order of .009 m/s. For a 0 dB signal-to-noise ratio, simulation points show that

$$\sqrt{M}\ SD\left(\frac{V_{est}}{2V_a}\right) \approx 0.2$$

where M is the number of pulses processed, v_{est} is the mean velocity estimate, and SD is the standard deviation. For M equal to 100, and v_a equal to 54.5 m/s, v_{est} is 2.2 m/s. Thus, a signal-to-noise ratio should be more than 0 dB to make reasonably accurate measurements of the mean Doppler velocity.

5.4.4 The Transmitted Waveform and Peak Power Requirements

Most weather radars do not use pulse compression because the reflectivity of storms is high enough so that pulse compression is not needed. Another consideration is the sidelobe problem. When pulse compression is used, there are always range sidelobes, and the sidelobes from a region of strong return could be mistaken for echoes in a region with low return. The situation is different, however, for radars which measure the return from clear air because the returns are so weak. With pulse compression, the signal-to-noise ratio can be increased without exceeding the maximum output power of the final amplifier stage in the transmitter. Transmitting a short pulse 66.7 nsec long will provide 10 m range resolution, but the peak power required to obtain an adequate signal-to-noise ratio would be unreasonably high.

FM-CW waveforms are often used in radars which measure wind profiles with beams pointed toward the zenith, because a high duty cycle can be obtained to increase the average power transmitted. A similar waveform, linear FM or chirp, would be appropriate for the ship wind sensor; Figure 5-5 and Figure 5-6 explain the principles of using a chirp waveform. The chirp generator on the left side of Figure 5-5 generates a signal whose frequency varies linearly with time and this pulse is transmitted toward a point target. The echo from the point target is received by a second antenna, and this echo mixes with the delayed version of the transmitted signal in a mixer. As shown in Figure 5-6, the mixer output is a pulsed sine wave. A bandwidth of 15 MHz will provide the required 10 meter range resolution.

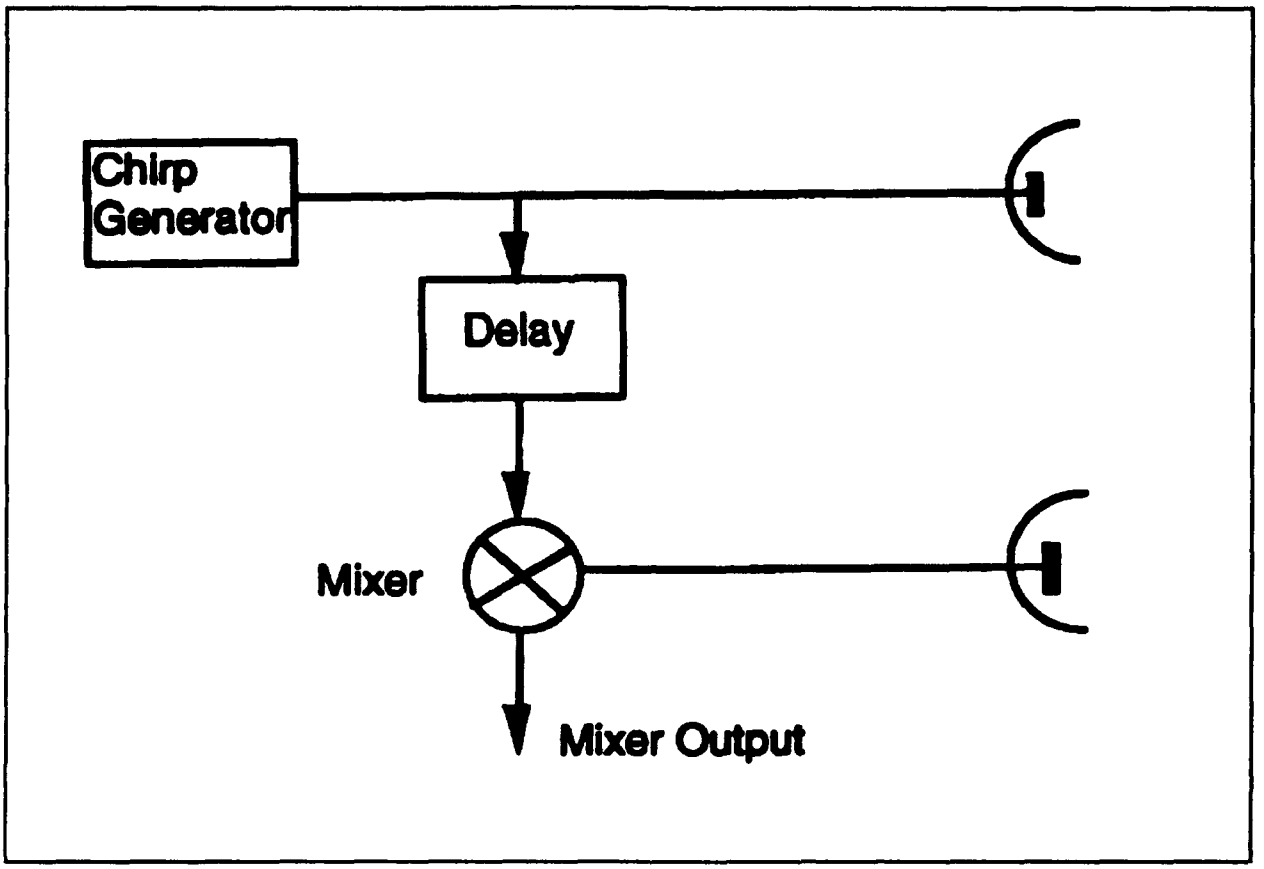

Figure 5-5. Simplified Block Diagram of Chirp Radar

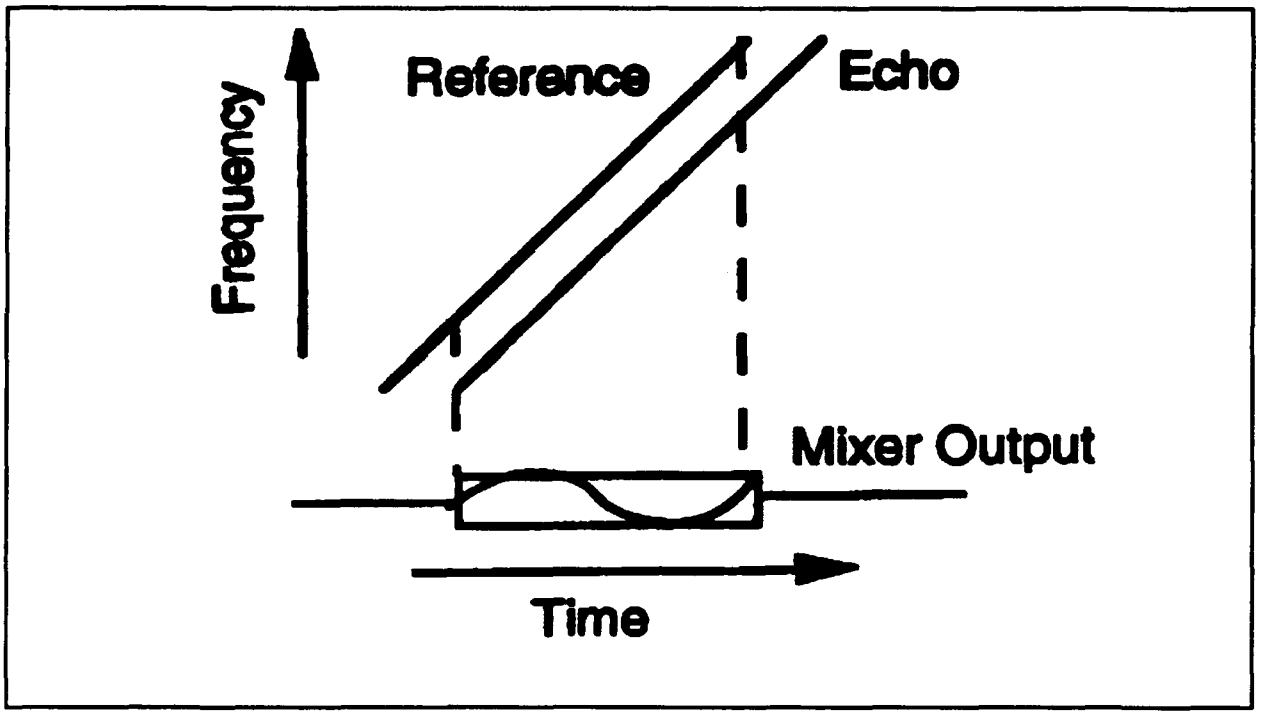

Figure 5-6. Point Target Response With Chirp Signal

Figure 5-7 is a sketch of the chirp waveforms for the wind sensor. The echoes from near range and the maximum range R_{max} of two kilometers have a time separation Δt of

$$\Delta t = \frac{2R_{MAX}}{c} = 13.3 \cdot 10^{-6} \text{sec}$$

As shown in below, the transmitted pulse length τ is the sum of the time separation and the recorded pulse length τ_{rec} because the start of the data recording is delayed by Δt until the beginning of the return from maximum range:

$$\tau = \Delta t + \tau_{rec}$$

Assuming that τ_{rec} is 100 μsec, the transmitted pulse length will be 113.3 μsec.
Having selected the chirp waveform, we are in position to compute the signal-to-noise ratio which takes pulse compression into account. The noise power equals the product of Boltzmann's constant, the system noise temperature T_{sys}, and the bandwidth B. Dividing P_r by N (see pg. 6) provides the signal-to-noise ratio; however, the signal-to-noise ratio increases by the

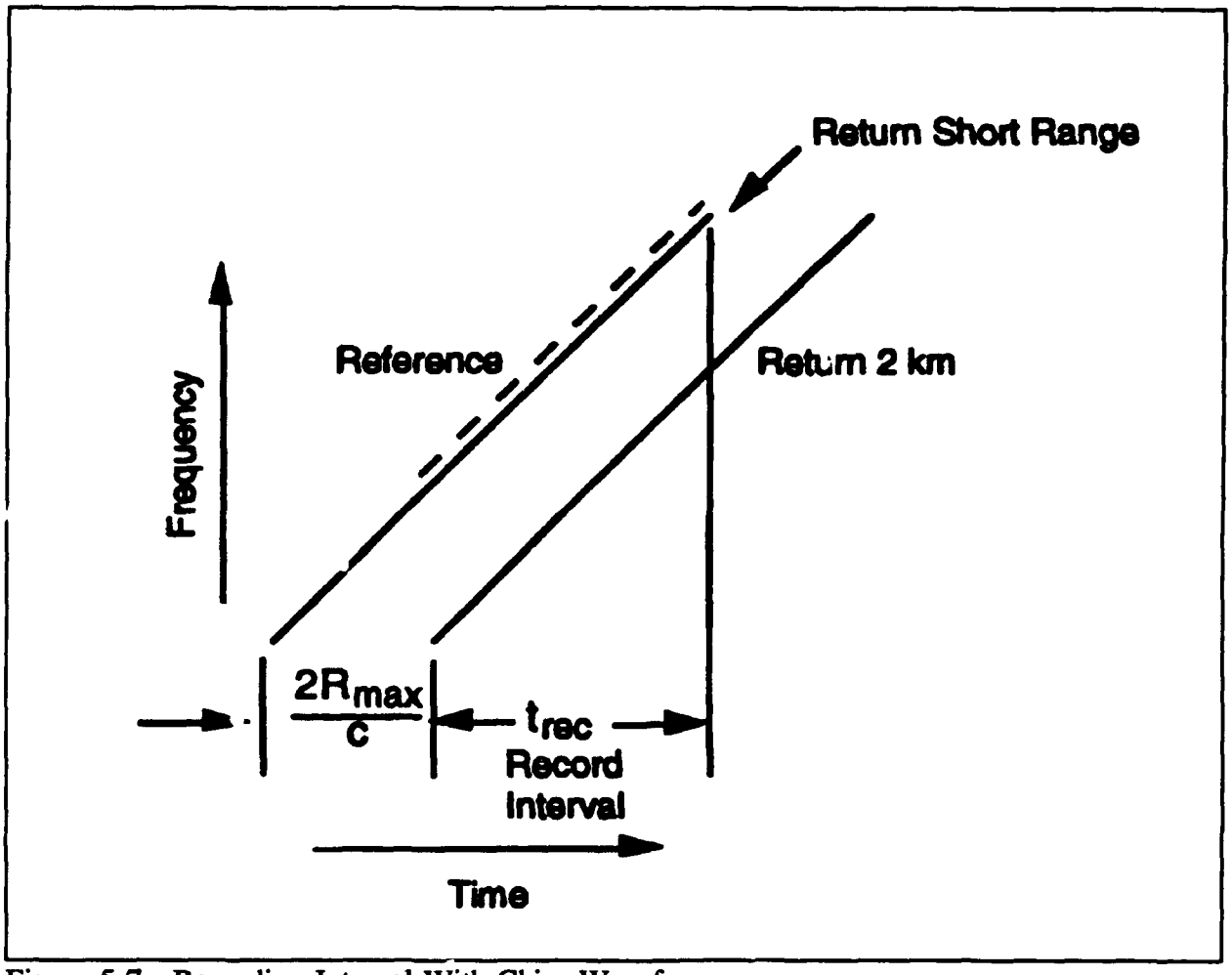

Figure 5-7. Recording Interval With Chirp Waveform

compression ratio, τ_{rec} B. We must also replace the resolution $c\tau/2$ for a standard pulse by ρ_r, the resolution with pulse compression. Hence, the signal-to-noise ratio for the wind sensor radar becomes:

$$S/Nr = \frac{P_t \tau_{rec} G^2 \lambda^2 \eta}{(4\pi)^3 R^2 L k T_{sys}} \cdot \frac{(\pi\theta^2)}{(8 \ln 2)} \rho_r$$

Typical parameters for the ship wind sensor are as follows:

P_t = 400,000 W, peak transmitted power

τ_{rec} = 100 μsec, recorded pulse length

G = 38.6 dB, antenna gain

λ= 0.0545 m, wavelength
η = 4x10-15 m^2/m^3, volume reflectivity of clear air
L= 4 dB, the sum of the RF and processing losses
k = 1.38 x 10-23 J/K, Boltzmann's constant
T_{sys} = 460 K, system noise temperature
θ = 35 mrad, 3 dB beamwidth of the antenna
ρ_r = 10 m, range resolution

The signal-to-noise ratio per pulse was computed using these parameters, and Figure 5-8 is a plot of the signal-to-noise ratio versus range. The signal-to-noise ratio is greater than the 0 dB minimum requirement for pulse-pair processing out to the maximum range of two kilometers; however, the peak power required is very high, 400 kW. Assuming a 113.3 μsec transmitted pulse length and a 4000 Hz PRF, the duty cycle is 45%, and the average power is 181 kW. A very powerful transmitter would be required to supply this amount of power.

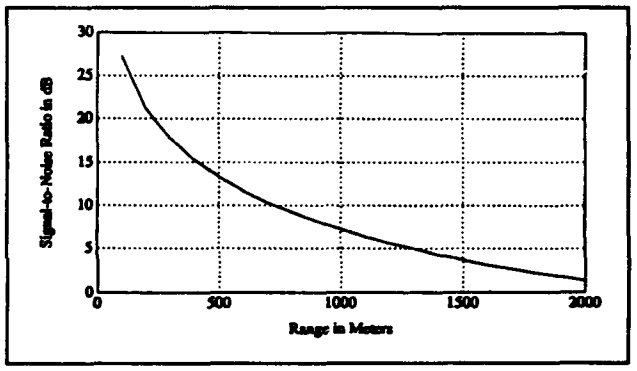

Figure 5-8. Signal-to-Noise Ratio Per Pulse for Wind Sensor

5.4.5 Clutter Suppression Requirements

The wind sensor will receive unwanted backscatter from the surface of the sea and from portions of the ship through the main beam and the sidelobes of the antenna. The residual clutter remaining after the application of clutter suppression techniques will limit the detectability of the faint returns from clear air. What is important is the ratio of the return power from clear air to the return power from the sea surface or the structure of the ship.

The signal-to-clutter ratio for the sea surface will be considered first. Let σ_{air} be the RCS of the return from a volume resolution cell of clear air; σ_{air} is proportional to the product of the reflectivity η of the cell, the volume of the cell, and the antenna gain G^2 at the cell

$$\sigma_{air} \propto \eta (R \cdot \theta)^2 \rho_r G^2$$

The relative RCS σ_{sea} of a resolution cell on the surface of the sea is proportional to the product of the reflectivity of the sea surface $\sigma_{o,}$ the area of the resolution cell, and the antenna gain G_C^2 in the direction of the sea surface. For small grazing angles

$$\sigma_{sea} \propto \sigma_o(R\theta)\rho_r G_c^2$$

The ratio of air RCS to sea RCS is the

$$\frac{\sigma_{air}}{\sigma_{sea}} = \frac{\eta R\theta}{\sigma_o}\left(\frac{G}{G_c}\right)^2$$

The reflectivity of the sea surface is a complex function of carrier frequency, sea state, wind direction, and the grazing angle; the reflectivity increases as the carrier frequency and grazing angle increase. The higher the sea state, the higher the reflectivity. If the radar is at a height of 20 meters, and the range is 1000 meters, the grazing angle is slightly over a degree. The table lists results for the required sea clutter suppression for sea states 1 through 5. Horizontal polarization has been used because the reflectivity is slightly less than for vertical polarization.

Sea State	σ_o (dBsm)	σ_{air} / σ_{sea} (dBsm)	Clutter suppression
1	-56	-22.6	32.6
2	-48	-30.6	40.6
3	-43	-35.6	45.6
4	-39	-39.6	496.
5	-36	-42.6	52.6

It may be difficult to achieve the 50 dB of clutter suppression required at the higher sea states in the presence of moving waves. The Terminal Doppler Weather Radar (TDWR) system operated by the Federal Aviation Administration for the detection of hazardous weather near air terminals requires 54 dB of clutter suppression to detect a 0 dBZ target at ten kilometers; however, TDWR testbed experience suggests that the clutter suppression actually achieved is 10

to 15 dB less because of low level clutter from moving targets. The signal processor subsystem of the WSD-88D weather radar achieves 30 to 50 dB of clutter suppression [5.15], and 30 to 50 dB of clutter suppression may not be adequate for a radar wind sensor at sea. Because the ratio is proportional to range, more clutter suppression is required at shorter ranges, where more than 50 dB of clutter suppression is needed.

The measurement of wind speed with discrete scatterers in the sidelobe region of the antenna will also be a problem. Suppose that there is a discrete scatterer with an RCS $\sigma_{clutter}$ in the antenna sidelobe region. The effective ratio of the RCS of the air to that of the scatterer equals the RCS ratio multiplied by the square of the relative antenna gains:

$$\frac{\sigma_{air}}{\sigma_{clutter}} = \frac{\eta(R\theta)^2\rho_r}{\sigma_{clutter}} \left[\frac{G}{G_c}\right]^2$$

Suppose that the wind speed over the flight deck of a carrier is being measured, and that a man is in the antenna sidelobes. A typical RCS for a man is 1 m2 or 0 dBsm. For η = 4x1015, R = 50 m, 0 = 35 mrad, Pr = 10, and G/G_C = 25 dB, the effective RCS ratio is -79 dB, and 89 dB of clutter suppression would be needed for a measurement. Thus, with typical antenna $^{-15}$, R sidelobes 25 dB down, it would be quite difficult to measure wind speed very close to the flight deck of a carrier.

5.4.6 Some Performance Limiting Factors

There are a number of factors which limit system performance if they are not given adequate attention. Several of these factors are discussed below.

Transmitter-Receiver Isolation

With the proposed chirp waveform and short range operation, reception and transmission will occur at the same time. As shown in Figure 5-5, the simplified block diagram of the system, there are separate antennas for transmission and reception. With a single antenna, the leakage power from the transmitter to the receiver through the duplexer would be too high, and the transmitter would saturate the receiver. With separate antennas, there is no duplexer, but

there will still be leakage from the transmitting antenna to the receiving antenna; this leakage is a severe problem that has been recognized for a long time. Although the transmitted signal will be used as a reference to deramp the returns, the signal path from the chirp generator to the first mixer in the receiver must be stable and have a flat frequency response. The leakage signal from the transmitting to the receiving antenna is unlikely to meet these requirements.

The peak transmitted power is 400 kW (86 dBm), and the power in the reference signal to the receiver mixer will be about 10 dBm. Since the leakage power between the antennas, or through other parts of the system, to the receiver input should be well below the 10 dBm reference signal, the leakage power should be much more than 100 dB below the transmitted power.

Transmitter and Receiver Instabilities

Transmitter-receiver instabilities and noise are an important factor in meeting system clutter suppression requirements. Small variations in the amplitude or phase of the return from clutter can result in components at the same Doppler frequencies as the desired returns from clear air. Clutter suppression filtering will not remove these clutter components which, if large enough, may dominate the clear air returns. Instabilities can result from the transmitter exciters, reference oscillators, timing jitter, and other factors.

Dynamic Range

In order to meet the clutter suppression requirements, the clutter returns and those from clear air must both be within the linear range of the A/D converter. The TDWR system handles the dynamic range problem by using a 12-bit A/D converter and gain control [5.16]. With the RMS noise set at about two levels of the A/D converter, the noise level is approximately 60 dB below A/D converter saturation. When the signal-to-noise ratio becomes more than 60 dB, a fast acting automatic gain control (AGC) circuit is needed to keep the input signal below A/D converter saturation.

Imbalance in I and Q Receiver Channels

The received signal is complex, and there will be inphase (I) and quadrature (Q) receiving channels at the receiver output. Imbalances in amplitude and a nonquadrature phase shift between channels creates an image spectrum which is symmetric to the actual spectrum. To suppress the image spectrum by 40 dB, the amplitude imbalance must be less than 2%, and the phase imbalance must be less than 1.2 degree.

Spectral Width and Mean Velocity of Sea Clutter

Weather radars are normally land based, and they have a clutter notch at dc to suppress ground returns. Although the Doppler spectrum of ground clutter is narrow, it has a finite width because vegetation moves in the wind, and target illumination changes as the antenna scans. The ground clutter spectrum can usually be removed with a filter notch width between 2 and 4 % of the Nyquist frequency. Suppressing sea clutter with a notch filter will be much more difficult than removing land clutter. Relatively few measurements of the microwave spectrum of sea clutter appear to be available so that there is some uncertainty on the spectral characteristics, and the scattering features of sea clutter are associated with several types of motion. The virtual Doppler velocity V_{vir} for the peak of the clutter spectrum for an X- or C-band radar looking upwind is [5.17]:

$$V_{vir} \approx 0.25 + 0.13 \cdot U \quad \text{m/s} \quad \text{(vertical polarization)}$$

or

$$V_{vir} \approx 0.25 + .18 \cdot U \quad \text{m/s} \quad \text{(horizontal polarization)}$$

Here U is the wind speed in meters per second. At look directions going away from up wind, the peak Doppler goes through a cosine dependence with zero Doppler at cross wind and negative Doppler downwind. The spectral width remains constant with the wind direction, but the spectral width of sea clutter is much wider than that of ground clutter. The ship itself will be in motion relative to the sea surface, and the antenna will be scanning. Constructing a clutter

suppression filter which can track the mean Doppler velocity with these changes and provide the required amount of clutter suppression is a high risk undertaking.

5.4.7 Range Ambiguities

The PRF for the ship wind sensor is high enough so that returns from ambiguous ranges will be superimposed on the desired return from short range. If R is the desired range, and η is the reflectivity at the desired range, the ratio of the power from the desired range to the power from the ambiguous range P/P_a is

$$\frac{P}{P_a} = \frac{\eta}{\eta_a}\left[\frac{R_a}{R}\right]^2$$

Here η_a is the reflectivity at the ambiguous range, and R_a is the ambiguous range which is the sum of R and n ΔR. Thus,

$$\frac{P}{P_a} = \frac{\eta}{\eta_a}\left[\frac{R + N\Delta R}{R}\right]^2$$

Here n is order of the ambiguity. With the anticipated 4000 Hz PRF, the unambiguous range interval is 37.5 kilometers. If the reflectivities of the air are the same at both ranges, the power ratio will depend only on the square of the ranges. The ratio will be the lowest at two kilometers, the longest operating range of the sensor. For the first ambiguity where n is 1, the ratio of the ranges is $(39.5/2)^2 = 390$ or 25.9 dB; for the second range ambiguity the ratio is 31.7 dB, and the power ratio will continue to decrease for higher order ambiguities.

Range ambiguities are troublesome only when the power from the overlaid range cells is more than 10 % of the power from the desired echo; consequently, range ambiguities will not cause problems when the reflectivity is the same at the desired range and the ambiguous ranges. Unfortunately, this will not always be the case, and the reflectivity at an ambiguous range can be much higher than that at the desired range when there is rain. In that case, it will not be possible to measure wind speed close to the ship.

5.4.8 Data Handling Requirements

The bandwidth of the received data after the mixer will be much less than the transmitted bandwidth because of the bandwidth reduction in the deramping process. The FM rate γ equals the bandwidth ΔB during the with recording time τ_{rec}

$$\gamma = \frac{\Delta B}{\tau_{rec}} = \frac{15 \cdot 10^6}{100 \cdot 10^{-6}} = 1.5 \cdot 10^{11} \text{ Hz/sec}$$

for the 15 MHz bandwidth and 100 μsec recording interval discussed previously. The deramped bandwidth Δ b is:

$$\Delta b = \frac{2\gamma \Delta r}{c} = 2 \text{ Mhz}$$

for a range interval Δr of 2000 m.

The sampling rate f_s must be 2 Δb or more to satisfy the Nyquist sampling criterion so that there is no aliasing of the data; a sampling rate of 5 MHz will be assumed. The number of samples recorded per pulse N_p equals the sampling rate times the recorded pulse width τ_{rec}

$$N_p = f_s \tau_{rec} = 5 \cdot 10^6 \cdot 100 \cdot 10^{-6} = 500$$

The data rate DR equals the product of the samples per pulse, the PRF, and the number of bits per sample word W_b. The A/D converter must have 12 bits for a wide dynamic range; hence,

$$DR = N_p \text{ PRF } W_b = 24 \text{ Mbits/s}$$

5.4.9 Sensor Design Summary

5.4.9.1 Block Diagram

Figure 5-9 is a much simplified block diagram of one possible wind sensor implementation based on the discussions above. As mentioned previously, there will be separate antennas for transmission and reception to help isolate the transmitter from the receiver. There will be two exciters, one for the transmitter and one for the receiver, which provide the transmitted and

reference chirp waveforms. The reference waveform will be offset from the transmitted waveform by the IF center frequency; there must, of course, be phase coherence between the two waveforms. The transmitting and receiving antennas will be aligned so that their beams are parallel, and they will be mounted on the same pedestal so that they can be scanned as a pair.

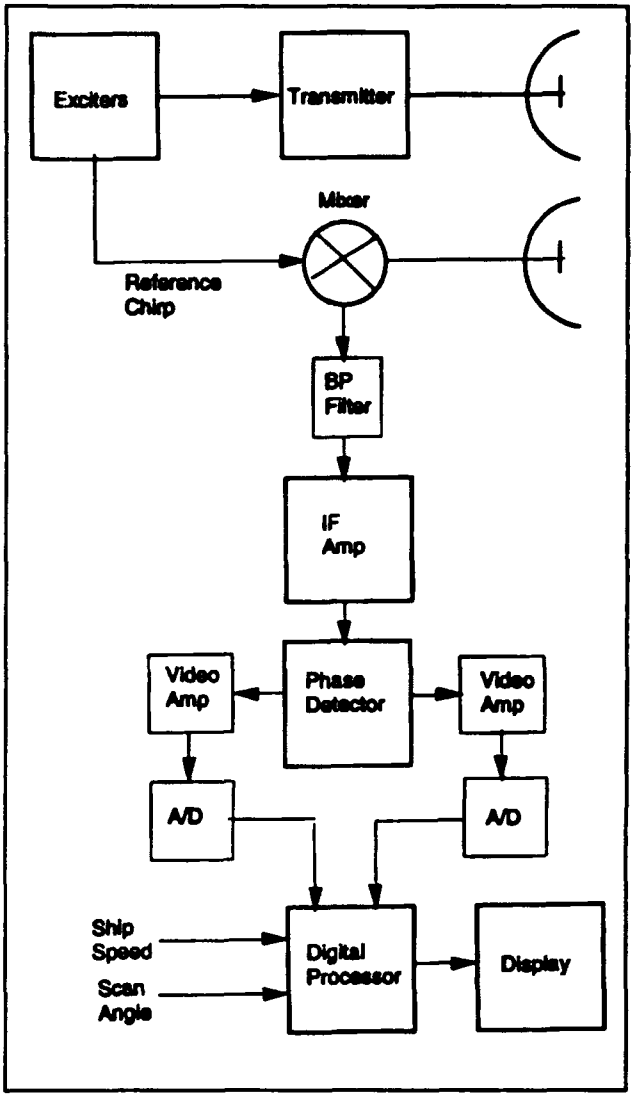

Figure 5-9. Simplified Block Diagram of Wind Sensor

The reference chirp will mix with the received echoes in the mixer connected to the receiving antenna, and the mixer output will go to a bandpass filter which will remove echoes outside the 50 to 2000 meter measurement range. One of the outputs from the band pass filter goes to the IF amplifier and the other to circuitry which provides automatic gain control for the IF amplifier to keep the receiver operating in its linear dynamic range. The IF amplifier output passes to a phase detector whose other input is a reference signal whose frequency equals the IF center frequency; the phase detector outputs are the I and Q video signals.

The I and Q video signals are digitized in separate A/D converters, and these signals pass to the processor. The digital processor will take an FFT to compress each pulse in range. Other inputs to the processor will be the ship's speed and the scan angle of the antennas; this data will be used in computations to determine the mean Doppler frequency in each resolution cell so that notch filtering can be used to suppress the sea clutter in the cell. After the sea clutter has been notched out, pulse pair processing will be applied to measure the Doppler in the resolution cell.

5.4.9.2 Parameter Summary

Figure 5-10 lists some of the key wind sensor parameters which were derived above; additional study would be necessary to provide a complete parameter list. One of the key system parameters is the antenna sidelobe level: the antenna sidelobes must be low and the elevation angle must be high enough to minimize the sea clutter return from the ocean surface. The wind sensor requires a very high power transmitter to detect the faint backscattered signals from clear air: a peak power of 400 kW would require a very large and expensive transmitter which would not be very suitable for a shipborne environment.

Search Volume	
Environment	Clear Air
Range	50 to 2000 m
Range Resolution	10 m
Angular Resolution	2 degrees
Minimum Elevation Angle	2 or 3 degrees
Height	10 to 100 m
Primary Angular Coverage	90 degree Arc at Stern
Secondary Angular Coverage	360 degrees
Scan Rate	9 degrees/s
Antennas	
Approach	2 Identical Antennas for Transmission and Reception
Isolation between Antennas	> 100 dB
Polarization	Linear
Reflector Diameter	1.56 m
Gain	38 dB
Beam Width	2 degrees
First Sidelobe	25 dB
Transmitter	
Frequency	5.5 GHz
Peak Power	400 kW
Average Power	181 kW
Waveform	Linear FM (Chirp)
Pulse Width	113.3 μsec
FM Rate	1.5×10^{11} Hz/s
PRF	4000 Hz
Duty Cycle	45.3%
Range Resolution	10 m
Receiver	
Noise Temperature	460 K
Losses	4 dB
Band Width	1 MHz
A/D Converter	12 bits
A/D Sampling Rate	5 MHz
Signal Processor	
Data Samples/Pulse	500
Data Rate	24 Megabits/s
Clutter Suppression	50 dB Required
Algorithm	Pulse-Pair Processing
Wind Measurement Accuracy	1 m/s goal

Figure 5-10. Key Wind Sensor Parameters

A complex signal processor is required to successfully measure wind speed near ships in the presence of sea clutter. The algorithms presently in use for landbased weather radars notch out ground clutter at zero Doppler frequency, but the mean frequency of the sea clutter spectrum will vary with the ship speed, the direction of the wind, and the scan angle of the radar. Coping with these variables will make it much more difficult to get the required 50 dB of clutter suppression at sea.

5.4.9.3 The Radiation Hazard

The extremely high power radiated by the transmitter presents a severe radiation hazard for anyone who might be in or near the main lobe of the radar antenna. The power level which the American National Standard Institute (ANTI) recommends for human exposure to electromagnetic fields in the 1.5 to 100 GHz region is 5 mW/cm^2; the power density is to be

averaged over a six minute period [5.18]. The power in the main lobe of the transmitting antenna will exceed the recommended exposure level by an order of magnitude. At a range of 100 meters, the area of the main lobe of the two degree antenna beam will be about 10 m^2. If the 180 kW average power of the transmitter were uniformly distributed over the 10 m^2, the power density would be 18 kW per square meter or 180 mW/cm^2. Hence, anyone in the main beam of the antenna would be exposed to a power level over 30 times the level recommended for human exposure. Thus, measurements of wind speed near the flight deck of a carrier would present a serious radiation hazard for personnel. There would still be a radiation hazard if the radiated power were reduced by a factor of ten.

5.5 REFERENCES

[5.1] R.J. Doviak and D.S. Zimic, Doppler Radar and Weather Observations, Academic Press, Orlando, 1984.

[5.2] Nathanson, Radar Design Principles 2nd Ed., Ch. 14, McGraw-Hill, New York.

[5.3] R.J. Serafin, "Meteorological Radar", in Radar Handbook, 2nd Ed., L.M. Skolnik, Ed., Ch. 23, McGraw-Hill, New York, 1990.

[5.4] W.H. Heiss, D.L. McGraw, and D. Sirmans, "NEXRAD, Next Generation Weather Radar (WSR-88D)," Microwave Journal, Vol. 33, No. 1, pp. 79-98, January 1990.

[5.5] M. Michelson, W.W. Shrader, and J.G. Wieler, "Terminal Doppler Weather Radar," Microwave Journal, Vol. 33, No. 2, pp. 139-148, February 1990.

[5.6] J. Rottger and M.F. Larsen, "UHF/VHF Radar Techniques for Atmospheric Research and Wind Profiler Applications," in Radar in Meteorology; Battan Memorial and 40th Anniversary Radar Meteorology Conference, D.Atlas, ed., pp. 235-281, 1990.

[5.7] Mr. Michael Jones, private communication.

[5.8] J. Evans and D. Turnbull, "Development of an Automated Windshear Detection System Using Doppler Weather Radar," Proc. IEEE, Vol. 77, No. 11, pp. 1661-1673, November 1989.

[5.9] R.R. Rodgers, et. al, "Radar Reflectivity of the Clear Air at Wavelengths of 5.5 and 33cm," Radio Science, Vol. 27, No. 5, pp. 645-659, September-October 1992.

[5.10] E.E. Gossard, "Refractive Index Variance and Its height Distribution in Different Air Masses," Radio Science, Vol. 12, No. 1, pp. 89-105, 1977.

[5.11] M.C. Thompson, F.E. Marbr and K.C. Allen, "Measurement of the Microwave Structure Constant Profile," IEEE Trans. on Antennas and Propagation, Vol. 28, No. 2, pp. 279-280, March 1980.

[5.12] E.L. Andreas, "The Refractive Index Structure Parameter, C_n^2, for a Year Over the Frozen Beaufort Sea," Radio Science, Vol. 24, No. 5, pp. 667-679, September-October 1989.

[5.13] R. Lhermitte, "A 94-GHz Doppler Radar for Cloud Observations," Journal of Atmospheric and Oceanic Technology, Vol. 4, pp. 36-48, 1987.

[5.14] D.D. Aalfs, E.G. Baxa and E.M. Bracalente, "Signal Processing Aspects of Windshear Detection," Microwave Journal, Vol. 36, No. 9, pp. 76-96, September 1993.

[5.15] W.K. Saunders, "FM and CW Radar," in Radar handbook, 2nd Ed., M. Skolnik, Ed., Ch. 14, McGraw-Hill, New York, 1990.

[5.16] J.E. Evans, et. al, "Terminal Doppler Weather Radar Clutter Control," IEEE International Radar Conference Proc., 1992.

[5.17] L.B. Wetzel, "Sea Clutter," in Radar Handbook, M. Skolnik, Ed., Ch. 13, McGraw-Hill, New york, 1990.

[5.18] E.C. Jordan, Reference Data for Radio Engineers, 7th Edition, P. 48-53, Howard W. Sams & Co., 1985.